University of Windsor

Scholarship at UWindsor

Electronic Theses and Dissertations

Theses, Dissertations, and Major Papers

2008

Laminar flamelet modeling of pilot jet methane/air flames

Pusheng Zhang
University of Windsor

Follow this and additional works at: https://scholar.uwindsor.ca/etd

LAMINAR FLAMELET MODELING OF PILOT

JET METHANE/AIR FLAMES

By
Pusheng Zhang

A Thesis
Submitted to the Faculty of Graduate Studies through the Department of
Mechanical, Automotive and Material Engineering
in Partial Fulfillment of the Requirements for
the Degree of Master of Applied Science at the
University of Windsor

Windsor, Ontario, Canada

2008

Canada

DECLARATION of CO-AUTHORSHIP/PREVIOUS PUBLICATION

I. Co-Authorship Declaration

I am aware of the University of Windsor Senate Policy on Authorship and I certify that I have properly acknowledged the contribution of other researchers to my thesis, and have obtained written permission from each of the co-author(s) to include the above material(s) in my thesis.

I certify that, with the above qualification, this thesis, and the research to which it refers, is the product of my own work.

II. Declaration of Previous Publication

This thesis includes one original paper that has been previously published/submitted for publication in peer reviewed conference, as follows:

Thesis Chapter	Publication title/full citation	Publication status*
Chapter 3, 4	Pusheng Zhang, David S-K Ting and Purna Kaloni, "Laminar Flamelet Modeling of Pilot Jet Methane/Air Flame: Skeletal versus Detailed Mechanisms" CSME, 2008	Published

I certify that I have obtained a written permission from the copyright owner(s) to include

the above published material(s) in my thesis. I certify that the above material describes work completed during my registration as a graduate student at the University of Windsor.

I declare that, to the best of my knowledge, my thesis does not infringe upon anyone's copyright nor violate any proprietary rights and that any ideas, techniques, quotations, or any other material from the work of other people included in my thesis, published or otherwise, are fully acknowledged in accordance with the standard referencing practices. Furthermore, to the extent that I have included copyrighted material that surpasses the bounds of fair dealing within the meaning of the Canada Copyright Act, I certify that I have obtained a written permission from the copyright owner(s) to include such material(s) in my thesis.

I declare that this is a true copy of my thesis, including any final revisions, as approved by my thesis committee and the Graduate Studies office, and that this thesis has not been submitted for a higher degree to any other University or Institution.

ABSTRACT

Nonpremixed turbulent combustion is a prevalent phenomenon in many practical applications. Theoretical research like simulating a well quantified piloted methane/air jet flame can serve as a means to make this technology effective, economical and clean. In this work, a Masri-Bilger piloted methane/air jet flame has been modeled by invoking the laminar flamelet assumption in FLUENT. The purpose was to investigate the effects of chemical reaction mechanisms and scalar dissipation rates on the accuracy of the model. Smooke's skeletal mechanism with 17 species and 25 reactions has been compared with GRI-Mech 3.0, a detailed mechanism consisting of 53 chemical species and 325 elementary reactions. The scalar dissipation rate was varied from 0.001 to $20 \, s^{-1}$. The results confirm the ability of the steady laminar flamelet model in qualitatively predicting the non-premixed, turbulent jet flame in terms of temperature and species profiles. The inclusion of detailed chemistry only led to marginally improved prediction. Scalar dissipation rate has a more pronounced influence on the predicted results, indicating that an appropriate nonzero dissipation rate is needed to better capture the underlying physics.

To my respectable parents
and my beloved wife

ACKNOWLEDGEMENTS

TABLE OF CONTENTS

LIST OF TABLES

LIST OF FIGURES

NOMENCLATURE

a_s	Strain rate [s^{-1}]
c_i	Concentration of species i
$C_{1\varepsilon}, C_{2\varepsilon}, C_{3\varepsilon}, C_d, C_g$	Model constants
C_p	Heat capacity [$J \cdot mol^{-1} \cdot K^{-1}$]
d	Diameter of the fuel jet [m]
D	Diffusion coefficient
Da	Damköhler number
f	Mixture fraction
f_1, f_2	Mixture fraction in the tangent direction
$\overline{f'^2}$	Mixture fraction variance
f_{st}	Stoichiometric mixture fraction
F_x, F_y, F_z	Body forces in the x, y and z directions [N]
G_b	Generation of kinetic energy due to mean velocity gradient
G_k	Generation of kinetic energy due to buoyancy
h	Enthalpy [J]
J_j^h	Enthalpy diffusion term
k	Kinetic energy [J]
k_{bj}	Backward reaction rate constant
k_{fj}	Forward reaction rate constant

Le_i	Lewis number of species i
p	Pressure [Pa]
Pr	Prandtl number
r	Radial distance from the flame center [m]
Re	Reynolds number
R_0	Radius of the fuel jet inlet [m]
Sc_k	Schmidt number
Pr	Prandtl number
t	Time [s]
T	Temperature [$^\circ$C]
$\bar{u}$	Velocity vector [m/s]
v_{ij}'	Stoichiometric coefficient of the ith species in the jth elementary reaction at the reactant side
v_{ij}''	Stoichiometric coefficient of the ith species in the jth elementary reaction at the product side
x	Direction along the x axis [m]
y	Direction along the y axis [m]
Y_i	Mass fraction of certain species
z	Direction along z axis [m]
Z_i	Elemental mass fraction for element i
Z_{oxy}	Oxidizer mass fraction

| Z_{fuel} | Fuel mass fraction |

Greek symbols

δ_{ij}	Kronecker symbol
ε	Dissipation rate
λ	Thermal diffusivity
μ	Laminar viscosity $[\,kg/(m \cdot s)\,]$
μ_{eff}	Effective viscosity $[\,kg/(m \cdot s)\,]$
μ_t	The turbulent viscosity $[\,kg/(m \cdot s)\,]$
ρ	Density $[\,kg/m^3\,]$
$\sigma_k, \sigma_\varepsilon$	Turbulent Prandtl number for k and ε
σ_t	Model constant
τ_{ch}	Chemical reaction time scale [s]
τ_t	Turbulent transport time scale [s]
ϕ	Scalar quality
$\bar{\phi}$	Density-weighted mean ϕ
χ	Scale dissipation rate $[\,s^{-1}\,]$
χ_{st}	Scale dissipation rate at stoichiometric mixture fraction $[\,s^{-1}\,]$
$\dot{\omega}_i$	Chemical reaction rate $[\,s^{-1}\,]$

Abbrevations

CPU   Central processing unit

DNS   Direct Numerical Simulation

LES   Large Eddy Simulation

MTOE   Million Tons of Oil Equivalent

RAM   Random access memory

RANS   Reynolds Averaged Navier Stokes

RSM   Reynolds Stress Model

SIMPLE   Semi-implicit method for pressure-linked equation

SLFM   Steady Laminar Flamelet Model

CHAPTER 1

INTRODUCTION

Nonpremixed (diffusion) combustion is a process when fuel and oxidizer enter separately into the combustion chamber where they mix and burn. This phenomenon is prevalent in engineering applications such as furnaces, diesel engines and aircraft gas turbine engines. As reducing emissions, conserving fuels, and raising efficiency of energy are becoming increasingly important, it is necessary to further improve existing energy conversion technology. With the increasing power of computational facilities, one promising way to achieve the improvement of the technology is by doing numerical simulations, which will help to improve and optimize the application in industries.

Numerical simulations, or Computational Fluid Dynamics (CFD), are very useful in predicting what will happen under a given set of circumstances. If carried out properly, its results can satisfy most industrial applications. In addition, simulations have the advantages to be relatively cheap and convenient when compared to experiments. For the simulation of nonpremixed turbulent combustion, the intense interaction between turbulence and chemistry is extremely complicated and thus, poses a real challenge for numerical modeling. Over the last couple of decades, there have been serious efforts invested in advancing our numerical modeling skill and capability. Some models, which have received much attention, include the laminar flamelet model [Peters, 1986], the PDF

transport model [Pope, 1985], and the conditional moment closure model (CMC) [Bilger, 1993]. The most promising approach emerged from this endeavor appears to be laminar flamelet modeling, which treats a turbulent flame brush as an ensemble of discrete, laminar flame elements (or laminar flamelets).

Laminar flamelet modeling of nonpremixed turbulent combustion is still an incompletely explored topic. The complicated chemical kinetics and the intricate interaction of the turbulence and the chemistry are solved partially, but never completely. To get a better understanding and improve the accuracy of the model, systematic investigation of different parameters of the model is indispensable.

1.1 Objective

This study aims at investigating the accuracy of the simplified model by evaluating the roles of chemical mechanisms and scalar dissipation rates in modeling a Masri-Bilger pilot jet methane/air nonpremixed flame [University of Sydney, 1984]. Particularly, a simple reduced mechanism, Smooke's skeletal mechanism consisting of 17 species and 25 reactions [Smooke, 1991], is compared with the more comprehensive GRI-Mech 3.0 mechanism with 53 species and 325 reactions [Smith et al., 2000]. To account for the slowing down of local reaction due to straining, the scalar dissipation rate is varied from 0.001 to 20 s^{-1}.

1.2 Scope of the Thesis

To achieve these objectives, the k-ε model coupled with the steady laminar flamelet model (SLFM) is used. We start by introducing the mathematical formulation, where flamelet equations are built and essential concepts such as mixture fractions, probability density function and scalar dissipation rate are brought in and formulated. Two types of chemical mechanisms are adopted, a skeletal chemical mechanism with 17 species and 25 reversible reactions and a detailed mechanism, a GRI-Mech 3.0 mechanism, consisting of 53 chemical species and more than 325 elementary reactions. The model is run under scalar dissipation rates of 0.001, 10 and 20 s^{-1}. The numerical results are compared with the experiment from the University of Sydney.

1.3 Outline of the Thesis

In Chapter 2, the background and the classification of turbulent combustion are given. The feasibility of the laminar flamelet model to simulate nonpremixed combustion is discussed. Chapter 3 focuses on the theoretical formulas. Some fundamental concepts of the non-reacting flow and reacting flow are given. In Chapter 4, the Masri-Bilger piloted methane/air jet flame is simulated in different cases by SLFM. These results are discussed in physical domain for scalar quantities, such as temperature and species. Particular emphasis is on how the simulated results compare with experiment. Finally, conclusions from this study are given in Chapter 5. Also, some recommendations for the future work are provided.

CHAPTER 2

LITERATURE REVIEW

2.1 Background

Energy plays an essential role in our lives. Currently, energy is the main factor to propel the development of society and economy. Energy is used in different forms to meet the basic need of human being such as cooking, lighting, heating, cooling, and transportation. It is also indispensable in all segments of industries. Figure 2.1 shows that the world primary energy is supplied by fossil fuels, mainly oil, gas and coal (MTOE stands for Million Tons of Oil Equivalent). One method to release energy from those fuels is via combustion. In part this is the reason that so many researches are being conducted on improving the efficiency and reducing the emission of combustion.

2.1.1 Classification of Turbulent Combustion

There are several ways to categorize combustion. The most common way is based on how the fuel is supplied into the reaction zone. Accordingly, combustion is classified into two categories: premixed combustion and nonpremixed combustion. For premixed combustion, fuel and oxidizer are mixed at the molecular level before the mixture is ignited. The prime example is the combustion process in spark-ignition engines. In contrast, nonpremixed turbulence combustion is a process when fuel and oxidizer enter separately into the combustion chamber where they mix and burn during continuous

interdiffusion [Rogg et al., 1986]. The study of this thesis will focus on the latter category.
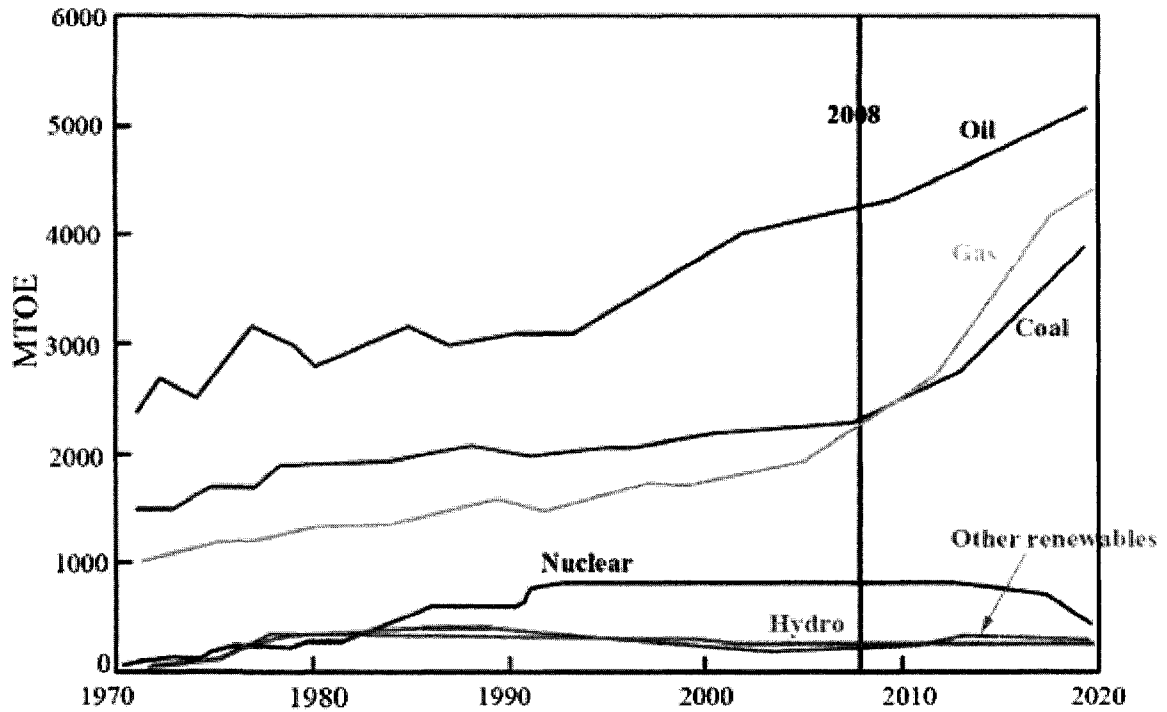
Fig. 2.1 World primary energy supply by fuel (1971-2020) [IEA, 2001].

2.1.2 Regimes of Nonpremixed Combustion

Nonpremixed combustion is widely used in diesel engines, liquid fueled gas turbines, furnaces and fires. To understand the feasibility of the laminar flamelet model to simulate nonpremixed combustion, we need to be aware of the regimes of nonpremixed combustion. The commonly utilized dimensionless number for this is the Damköhler number, which shows the importance of the interaction between chemistry and turbulence.

5

It is the ratio of the turbulent transport time scale (τ_t) and the chemical reaction timescale (τ_{ch}), that is

$$Da \equiv \frac{\tau_t}{\tau_{ch}} \qquad (2.1)$$

The Damköhler number (Da) and the Reynolds number (Re) can fully define a laminar diffusion flame. When Damköhler is small, the time scale of turbulence is short compared to the time scale of chemical reaction. Turbulence, thus, has enough time to alter the chemical reaction zone. Due to the relatively smaller eddy size and smaller mixing length than the reaction zone thickness, the intensity of the transport processes in the combustion front is enhanced, resulting in intense mixing and reaction. This regime is called the distributed reaction zones regime as shown in Figure 2.2. This regime is so complicated that none of the existing models can handle it in any satisfactory manner. If the chemical reaction is fast compared to mixing, the Damköhler number is large enough and the reacting flow may be treated as quasi-steady and the combustion is in the flamelet regime. When combustion is in a flamelet scenario, many existing theoretical models work well. In an ideal case, the large eddies only distort the smooth laminar flamelet front, but there is no effect on the reaction as portrayed in Figure 2.2. In reality, however, there is some alteration of the reaction, especially at higher Reynolds number. The present study only deals with the model in the flamelet regime.

Distributed reaction zones regime   **Flamelet regime**
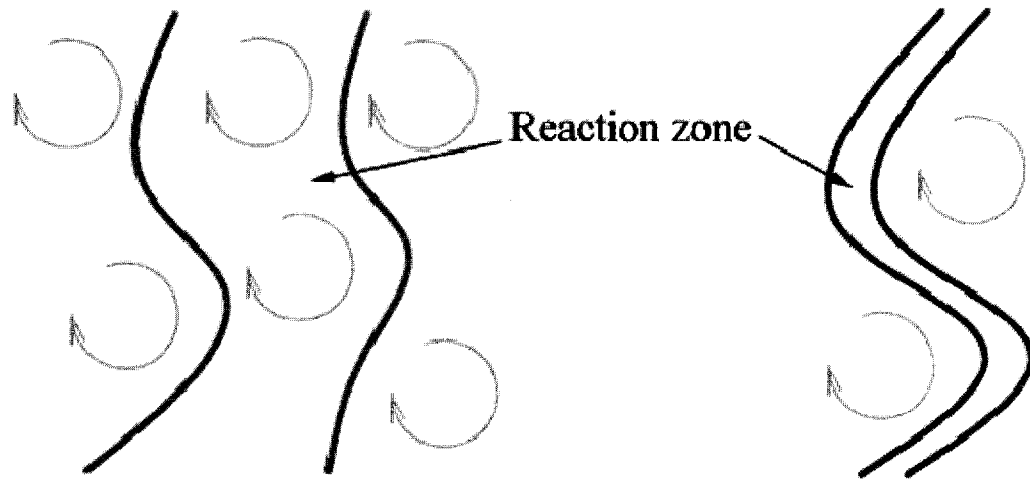
Reaction zone

Fig. 2.2 Effect of turbulence on the structure of the reaction zone.

A diagram for the nonpremixed laminar flames has been presented [Swaminathan, 2002] in Figure 2.3, which shows the regimes as function of the Damköhler number (Da), and the turbulent Reynolds number (Re). In the high Re case, when the chemistry is fast enough (large Da), the flame has flamelet structures. When Damköhler number is low, flame incline to extinguish. Between these two regimes, unsteady effect is pronounced.
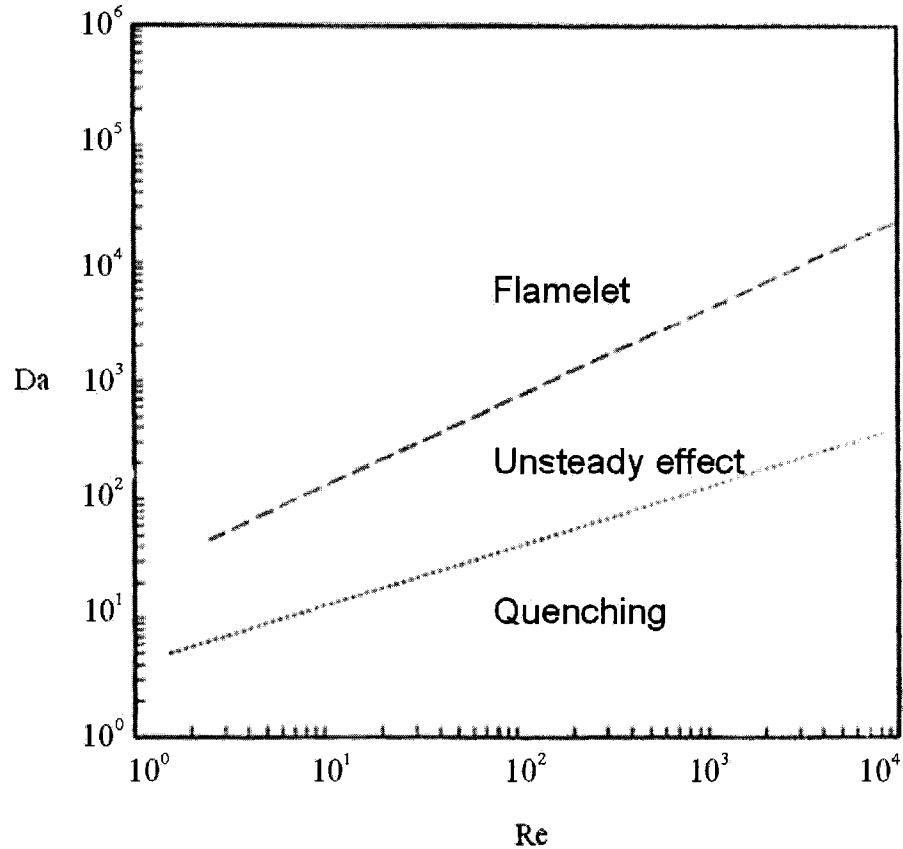
Fig. 2.3 Schematic demonstration of nonpremixed turbulent combustion regimes

[Swaminathan, 2002].

2.2 Flamelet Models and Chemical Mechanisms

Strictly speaking, the flamelet model is valid only in the flamelet regime. The flamelet

concept treats a diffusion combustion flame as an ensemble of laminar flamelets. Five

states of a diffusion flame have been identified by Peters [1984]. These are the steady

unreacted initial mixture, the unsteady transition after ignition, the quasi-steady burning

state, the unsteady transition after quenching and the unsteady transition after reignition.

2.2.1 Steady Laminar Flamelet Model

The basic idea of flamelet models is to treat the turbulent flames as an ensemble of laminar flamelets [Peters, 1984]. When we assume that the unsteady effects are not very pronounced and can be ignored, the model only needs to handle the first three states. In the present study, a steady-state assumption for the laminar flamelet is made to this model, the so-called steady laminar flamelet model (SLFM), so that the temperature and species of interest can only be the function of the mixture fraction and the scalar dissipation rate. This work will employ this model to simulate turbulent combustion. Relevant concepts and theoretical formula will be provided in Chapter 3.

2.2.2 Chemical Mechanisms

The flamelet approach is made feasible by decoupling the flow turbulence from the (simplified) chemistry. Many simplified reaction mechanisms have been devised over the years to make it practical for solving the methane/air diffusion combustion problem. These include the Kee mechanism which includes 18 species and 58 reactions [Peeters, 1995], Smooke skeletal mechanism consisting of 17 species and 25 reactions [Smooke, 1991] and Smooke-Puri-Seshadri mechanism with 17 species and 46 reactions [Smooke et al., 1986]. Recently, however, the accuracy of these reduced mechanisms in modeling nonpremixed combustion has been questioned [Skevis et al., 2007]. This is in part due to the significant advancement in computing power and the fact that different simplified mechanisms are only optimized for particular ranges of thermodynamic parameters such

as temperature and pressure. Nevertheless, for engineering applications in which time and money are two common constraints, simplified mechanisms will continue to play an important role. In other words, it is infeasible to enforce total versatility as this would require the inclusion of all possible species and reactions. Therefore, it is worth evaluating the various reduced and detailed mechanisms to ensure accuracy for the required application. This study aims at comparing the well recognized GRI-Mech 3.0 with the skeletal mechanism proposed by Smooke, when applied to simulating a pilot jet methane/air nonpremixed flame.

2.2.3 Scalar Dissipation Rate

Bilger [1988] suggested that portions of the turbulent flame under the influence of intense, fine-scale turbulence may be extinguished locally. With a small amount of straining, the initial increase in scalar dissipation rate signifies increased heat conduction from, and reactant diffusion to, the reaction zone; that is, the burning is enhanced. Straining beyond a critical value, however, can result in incomplete reaction and localized flame extinguishment caused by excessive heat loss which is not balanced by a corresponding heat gain. Thus, an appropriate nonzero mean scalar dissipation rate is needed for accurate modeling of a highly turbulent flame.

CHAPTER 3

GOVERNING EQUATIONS AND FLAMELET

MODEL FORMULATION

3.1 Governing Equations for Turbulent Reacting Flows

Motions and fluctuations take place in turbulent flows and generate some spatial structures, namely turbulent eddies. These eddies involve a wide range of time and length scales. The largest eddies mainly take the responsibility for effective mixing of mass, momentum and energy. During the development of the turbulent flow, it is commonly accepted that an energy cascade process translates the energy from the large eddies into the smaller eddies and causes variable time and length scales. In particular, the mean flow stretches and deforms the large eddies, while the conservation of angular momentum causes rotation. In this manner, the smaller eddies are formed. It is repeated until the smallest scales are dissipated by the action of the fluid viscosity. Those eddies with different time and length scales make the scenario very complicated and difficult to solve numerically. In reality, the largest length scale can be restricted in size by the system dimensions while the size of the smallest length scale is limited by the fluid viscous damping. In the case of reacting flow, the number of conservation equations increases proportional to the number of the chemical species. There can be hundreds of convection-diffusion equations when numerically simulating a turbulent combustion process, which include mass, momentum, energy and species equations.

11

Those equations are presented here.

3.1.1 Conservation Equations

The instantaneous continuity equation is written as

$$\frac{\partial \rho}{\partial t} + div(\rho \bar{u}) = 0 \qquad (3.1)$$

where ρ is the density, $\bar{u}$ is the velocity vector.

Based on the conservation law of mass, momentum and energy, the instantaneous

Navier-equations are written as:

Momentum in the three orthogonal dimensions:

x-momentum: $\qquad \frac{\partial(\rho u)}{\partial t} + div(\rho u \bar{u}) = -\frac{\partial p}{\partial x} + div(\mu \ grad \ u) + F_x \qquad (3.2)$

y-momentum: $\qquad \frac{\partial(\rho v)}{\partial t} + div(\rho v \bar{u}) = -\frac{\partial p}{\partial y} + div(\mu \ grad \ v) + F_y \qquad (3.3)$

z-momentum: $\qquad \frac{\partial(\rho w)}{\partial t} + div(\rho w \bar{u}) = -\frac{\partial p}{\partial z} + div(\mu \ grad \ w) + F_z \qquad (3.4)$

where p is the static pressure and F_x, F_y, F_z are body forces in the x, y and z directions,

respectively.

Total energy: $\qquad \frac{\partial}{\partial t}(\rho h) - \frac{\partial p}{\partial t} + \frac{\partial}{\partial x_j}(\rho u_j h) = \frac{\partial}{\partial x_j}(J_j^h + u_j \tau_{ij}) + u_j F_j \qquad (3.5)$

We assume that the gases that we are dealing with are Newtonian. The viscous tensor is

given as

$$\tau_{ij} = \mu_{eff} \left[\left(\frac{\partial u_i}{\partial x_j} + \frac{\partial u_j}{\partial x_i} \right) - \frac{2}{3} \delta_{ij} \left(\frac{\partial u_i}{\partial x_j} \right) \right] \tag{3.6}$$

where μ_{eff} is the effective viscosity, which yields from the summing up of the laminar (μ)

and turbulent viscosity (μ_t) and δ_{ij} is the Kronecker symbol. The enthalpy diffusion

term J_j^h is written as

$$J_j^h = -\frac{\mu}{Pr} \left[\frac{\partial h}{\partial x_j} + \sum_{k=1}^{N} \left(\frac{Pr}{Sc_k} - 1 \right) h \frac{\partial Y_k}{\partial x_j} \right] \tag{3.7}$$

The Prandtl number, Pr, is defined as $Pr = \mu_i \cdot C_p / \lambda$, where λ is the thermal diffusivity

and C_p is the constant pressure specific heat. Sc_k is the Schmidt number of the

k^{th} species defined as $Sc_k = \mu_1 / \rho \cdot D_k$, where D_k is the molecular diffusivity of the

species k and Y_k is the mass fraction of the species k.

3.1.2 Turbulence Modeling

The instantaneous continuity and Navier-Stokes equations (3.1-3.4) form a closed set of

four equations with four unknowns u, v, w and p. For turbulent flows, however, these

equations could not be solved directly because of the additional unknowns like the

Reynolds stresses. In this case, the main task of turbulence modeling is to develop

computational procedures with sufficient accuracy and generality, which engineers can

use to estimate the Reynolds stresses and the scalar transport terms. Detailed and recent

reviews are provided in Ferziger and Peric [1999] and Veynante and Vervisch [2002], for

examples. The following shows a brief summary of turbulent models.

a) Direct Numerical Simulation (DNS)

To get an accurate result, one way is to numerically solve the continuity and Navier-Stokes equations without any turbulence model. This means that the whole range of spatial and temporal scales of the turbulence must be resolved. In DNS, to describe all the significant structure of turbulence, the model has to involve the calculation domain as large as the largest turbulent eddy, which is on the order of integral scale. On the other hand, a valid simulation must also capture all the kinetic energy dissipation. The dissipation takes place primarily in the smallest dissipative scales, on which the viscosity is very active, so that the size of the grid goes all the way down to the viscously determined Kolmogorov scale. The results of DNS are very informative and can be treated as the "experimental" data. DNS, thus, is a useful tool in fundamental research in turbulence and it is extremely helpful in understanding the mechanisms of turbulence formation, energy transfer and the interaction of combustion and turbulence in reacting turbulent flows. However, the computational cost of DNS is extremely high, even at low Reynolds numbers. In most industrial applications, the computation of DNS would exceed the capacity of the most powerful computers currently available. Thus, the somewhat simplified 'DNS' such as the Reynolds Averaged Navier Stokes (RANS) and Large Eddy Simulation (LES) models come into existence.

b) Reynolds Averaged Navier Stokes (RANS) Model

The Reynolds Averaged Navier-Stokes (RANS) model becomes feasible for turbulence

modeling when all quantities are expressed as the sum of mean and the fluctuating parts
to build a closure approach. Then, the time average of the Navier-Stokes equations is
formed, where the equation system is closed and the number of additional equations for
turbulence quantities defines the type of turbulence model.

The standard k-ε two-equation turbulence model [Launder and Spalding, 1974] has been a
workhorse since 1980s. This model is a semi-empirical model and is characterized by
the turbulence kinetic energy (k) and its dissipation rate (ε). It is assumed that the flow
is fully turbulent and the effects of molecular viscosity are negligible during the
derivation of the k-ε model. The model, thus, only apply to fully turbulent flows. This
model will be used in this work.

For the turbulence kinetic energy (k) and its dissipation rate (ε), we have the transport
equations as [Launder and Spalding, 1974]:

$$\frac{\partial}{\partial t}(\rho k) + \frac{\partial}{\partial x_i}(\rho k \bar{u}) = \frac{\partial}{\partial x_i}\left[\left(\mu + \frac{\mu_t}{\sigma_k}\right)\frac{\partial k}{\partial x_i}\right] + G_k + G_b - \rho\varepsilon \tag{3.8}$$

and

$$\frac{\partial}{\partial t}(\rho\varepsilon) + \frac{\partial}{\partial x_i}(\rho\varepsilon\bar{u}) = \frac{\partial}{\partial x_j}\left[\left(\mu + \frac{\mu_t}{\sigma_\varepsilon}\right)\frac{\partial k}{\partial x_j}\right] + C_{1\varepsilon}\frac{\varepsilon}{k}(G_k + C_{3\varepsilon}G_b) - C_{2\varepsilon}\rho\frac{\varepsilon^2}{k} \tag{3.9}$$

Here the turbulent viscosity, μ_t, is computed by combining k and ε, that is

$$\mu_t = \rho C_\mu \frac{k^2}{\varepsilon} \tag{3.10}$$

where C_μ is a constant and is set equal to 0.09 by default, G_k is the generation of turbulence kinetic energy due to the mean velocity gradients, G_b represents the generation of turbulence kinetic energy due to buoyancy, $C_{1\varepsilon}$, $C_{2\varepsilon}$ and $C_{3\varepsilon}$ are constants and equal to 1.44, 1.92 and 1.53, respectively, σ_k and σ_ε are, respectively, the turbulent Prandtl number for k and ε and equal to 1.0 and 1.3. The above constants have been determined from experiments with air and water for fundamental turbulent shear flows including homogeneous shear flows and decaying isotropic grid turbulence.

c) Large Eddy Simulation Model (LES)

Large eddy simulation model operates by resolving the large eddies directly, while small eddies are modeled [Lesieur and Metais, 1996]. LES, thus, stands between DNS and RANS, since DNS directly resolve the entire spectrum of turbulent scales, while RANS models all the scales of the turbulence. By using the large eddy simulation model, much coarser mesh and larger time-steps sizes may be utilized compared to those in DNS. LES, however, basically uses finer meshes than those used for RANS calculations. Besides, to obtain stable statistics of the flow being modeled, LES has to be run for a sufficiently long flow-time. As a result, the computational cost involved with LES is normally orders of magnitudes higher than that for steady RANS calculations in terms of memory (RAM) and CPU time. Therefore, high-performance computing is a necessity for LES, especially for industrial applications.

16

3.2 Flamelet Model Formulation and Implementation

The flamelet concept treats a turbulent diffusion flame as an ensemble of diffusion flamelets by introducing a mixture fraction concept. Turbulence and chemistry are connected by presuming a Probability Density Function (PDF). It has a good coupling between the chemistry and the molecular transport.

3.2.1 Mixture Fraction

A primary (scalar) parameter utilized in (laminar) flamelet modeling is the mixture fraction. It is used to describe the mixing state of fuel and oxidizer. The effects of diffusion and convection, but not that of reaction, are directly accounted for via this conserved scalar [Peters, 2000]. The mixture fraction can be expressed [Sivathanu and Faeth, 1990] as

$$f = \frac{Z_i - Z_{oxy}}{Z_{fuel} - Z_{oxy}}$$

(3.11)

where Z_i signifies the elemental mass fraction for element i. The subscripts "fuel" and "oxy" stand for fuel and oxidizer; Z_{oxy} and Z_{fuel} denote the oxidizer mass fraction and fuel mass fraction, respectively, at the inlet. It is generally convenient to scale the mass fraction f from zero to one, where zero denotes pure oxidizer and one defines the pure fuel side [Bilger, 1980], as shown in Figure 3.1. In the special case where only a single diffusion coefficient and unity Lewis number apply, this concept simplifies the complicated thermochemistry into a simple mixing problem [Ferreira, 2001].

17
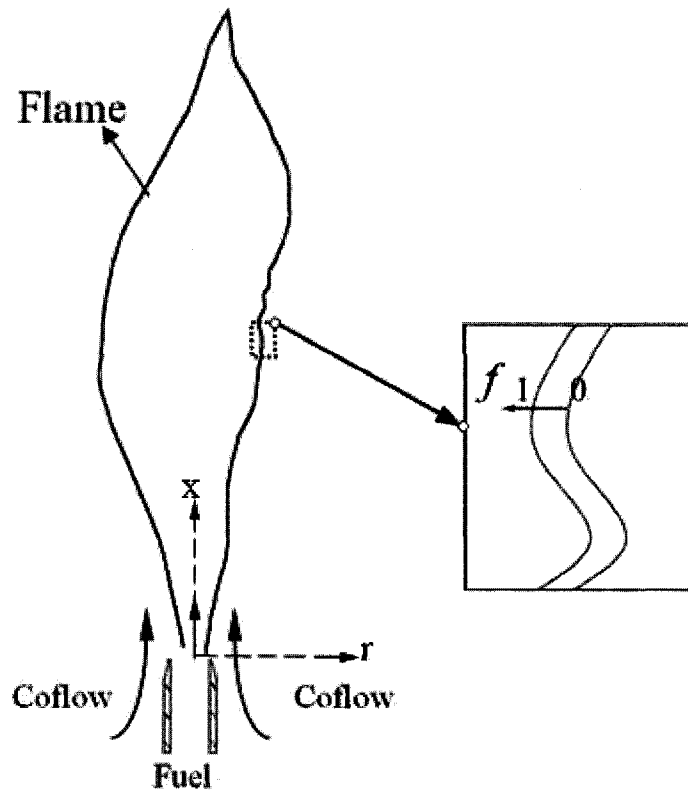
Fig. 3.1 Laminar flamelet structure.

3.2.2 Laminar Flamelet Generation

When the chemical time scale is much shorter than the flow turbulence time scale, the nonpremixed turbulent flame is in the laminar flamelet regime [Peters, 1986]. Under this condition, the fast chemistry forms a thin, though wrinkled, layer of reacting surface which may be visualized as a group of curved laminar flame surfaces (cusps) connected together (see Figure 3.1). These corrugated flame elements or laminar flamelets are so thin that they can be described by a set of one-dimensional governing equations.

The mass fraction of the chemical species and enthalpy are both conserved scalars, and thus, the corresponding thermo-chemical compositions in laminar and turbulent flows satisfy the transport equations,

$$\frac{\partial(\rho Y_i)}{\partial t} + div(\rho Y_i \bar{u}) = div\left(\rho D \nabla Y_i\right) + \dot{\omega}_i \qquad (3.12)$$

$$\frac{\partial \rho h}{\partial t} + div(\rho \bar{u} h) = div\left(\rho D \nabla T\right) + \frac{\partial p}{\partial t} \qquad (3.13)$$

Here Y_i signifies the mass fraction species i, ρ denotes density, $\bar{u}$ is the velocity vector, D is the diffusion coefficient, T is temperature, h stands for enthalpy and p represents pressure. The first term of Equation (3.12) indicates the rate of increase of Y_i within any fluid element. The second term shows the net rate of flow of Y_i out of the fluid element. The third term is the rate of increase of Y_i due to diffusion. The chemical source term $\dot{\omega}_i$ is the reaction rate of species i, which obeys the law of Mass Action, i.e.,

$$\dot{\omega}_i = \sum_j^J \left(v_{ij}'' - v_{ij}'\right)\left(k_{fj}\prod_i^I c_i^{v_{ij}'} - k_{bj}\prod_i^I c_i^{v_{ij}''}\right) \qquad (3.14)$$

where v_{ij}' and v_{ij}'' are the stoichiometric coefficients of the ith species in the jth elementary reaction for the reactants and products, respectively, c_i is the concentration of species i, k_{fj} and k_{bj} signify the forward and backward (reverse) reaction rate constants, respectively.

To simplify the model, a turbulent flame can be treated as an ensemble of discrete, laminar flame elements displaced, but otherwise unaffected, by flow turbulence. Then the flame structure can be analyzed on a small or local scale, one flamelet at a time. The

19

main reaction occurs around stoichiometric region, where iso-surfaces can be defined, for example, with respect to the mixture stoichiometry. For a two-stream case (one stream of oxidizer and one stream of fuel), a conservative scalar (parameter) known as mixture fraction can be introduced. The pure fuel side is typically assigned with unity mixture fraction, i.e., 100% fuel, and hence, the mixture fraction for the pure oxidizer side is zero. As a first step, we may assume that the diffusion coefficients for all species to be equal, simplifying the complex multi-component chemistry into a simple mixing problem. Transformation of Equations (3.12) and (3.13) can be conducted from physical spatial coordinate system to mixture fraction spatial coordinate system, i.e., from x, y, z to f, f_1, f_2 [Peters, 2000]. A sensible choice is to set mixture fraction f perpendicular to the surface element, with f_1 and f_2 (which signify pure fuel and pure oxidizer surfaces) parallel to the surface element (see Figure 3.1). In the new coordinate system, we can assume one dimensional behavior in the flame front and hence, f_1 and f_2 can be omitted. Consequently, the transport equations simplify into

$$\rho \frac{\partial (Y_i)}{\partial t} = \rho \frac{\chi}{2Le_i} \frac{\partial^2 Y_i}{\partial f^2} + \dot{\omega}_i \qquad (3.15)$$

$$\rho \frac{\partial T}{\partial t} + \sum_{i=1}^{N} h_i \dot{\omega}_i = \rho \frac{\chi}{2} \frac{\partial^2 T}{\partial f^2} + \frac{1}{c_p} \frac{\partial p}{\partial t} \qquad (3.16)$$

where Le_i is the Lewis number (heat diffusivity / mass diffusivity) for species i, c_p is the specific heat capacity at constant pressure, χ is the scalar dissipation rate, which represents the rate of scalar gradient, given as

20

$$\chi = 2D|\nabla f|^2 \tag{3.17}$$

For the methane/air flame considered in this study, we may further assume the corresponding Lewis number to be unity.

Scalar dissipation rate χ can be calculated at each location of the flow field via Equation (3.17). However, flamelet libraries are usually computed in advance and are assumed to be independent of the flow. In this case, the scalar dissipation rate cannot be taken from the flow field calculation, and has to be introduced as a scalar parameter. Therefore, the scalar dissipation rate has to be modeled.

One way to study nonpremixed turbulent combustion is to treat the flame structure as a collection of strained counterflow diffusion flames, such as the one portrayed in Figure 3.2 [Dixon-Lewis, 1990; Bray and Peters, 1994]. This approach gives the relationship of the strain rate and the scalar dissipation rate by

$$\chi_{st} = f(f) = \frac{a_s}{\pi} \exp\{-2[erfc^{-1}(2f_{st})]\} \tag{3.18}$$

Here χ_{st} is the scalar dissipation at stoichiometric mixture fraction f_{st}, a_s is strain rate, $erfc^{-1}$ is the inverse complementary error function. The relationship between χ and χ_{st} is given as

$$\chi = \chi_{st} f(f) / f(f_{st}) \tag{3.19}$$

In this work, the scalar dissipation rate is assumed that the effects of flame stretching can be characterized by the single parameter χ_{st}, because most of the chemistry occurs near $f = f_{st}$ in the diffusion flame.
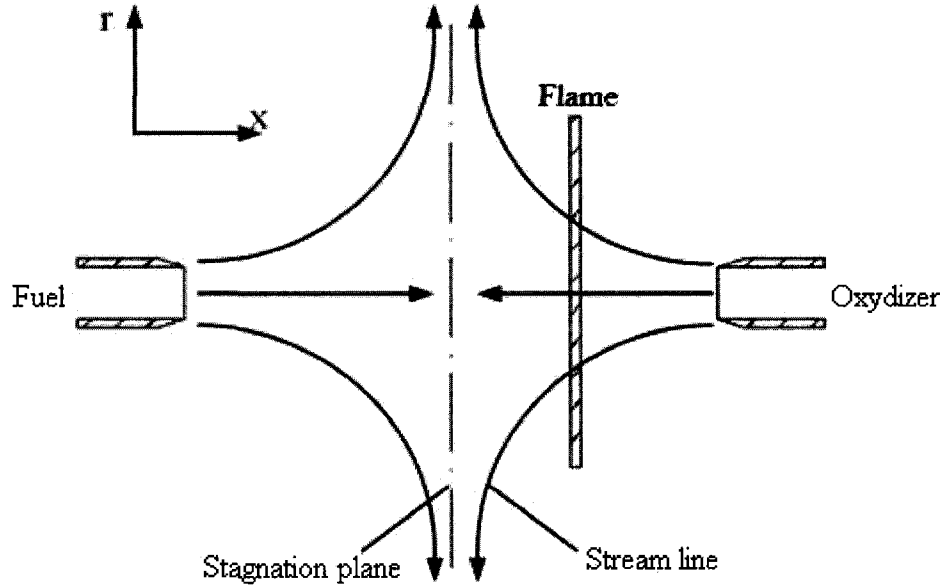
Fig. 3.2 Schematic diagram showing a typical counterflow, twin-flame configuration.

In the presence of turbulence, the flame surface is subject to fluctuations. These fluctuations can be described statistically via the mixture fraction f in terms of the mean mixture fraction $\bar{f}$ and its variance $\overline{f'^2}$. In other words, the effect of turbulent can be described by the statistical method called the probability density function (PDF). One can infer from the analysis above that the scalars of interest (including PDF) are only functions of $\bar{f}$, $\overline{f'^2}$, and χ_{st}.

3.2.3 Probability Density Function (PDF)

Beyond a certain Reynolds number the flow turbulence may alter the value of the mixture

fraction of species substantially.   The PDF approach has shown promise in dealing with

this turbulence influence.
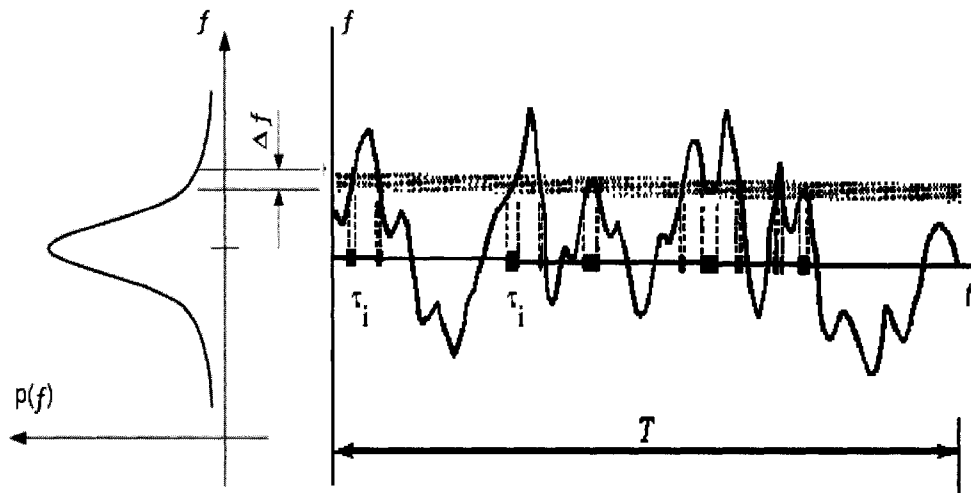
Fig 3.3 Schematic description of the probability density function

[FLUENT 6.2 User's Guide].

As shown in Figure 3.3, PDF is a statistical tool devised to model the effect of turbulence

on chemistry.   It can be treated as the fraction of time that the fluid spends at the state f .

On the right side of the figure, the fluctuating value of f spends some fraction of time in

the range, which is denoted as $\Delta f \cdot p(f)$.   It is plotted on the left side of the figure,

which takes on values such that the area under its curve in the band denoted, Δf , is equal

to the fraction of time that f spends in this range, given mathematically,

$$p(f)\Delta f = \lim \frac{1}{T} \sum_i \tau_i \qquad (3.20)$$

here T is the time scale and τ_i is the amount of time that f spends in the Δf band. The argument behind this approach is that the time averaged values are capable of providing useful information, that is, better than tracing the ever fluctuating instantaneous quantities which tend to overload our data acquisition capabilities. By invoking the statistical averaging method, we can deduce the mean values of conserved scalars via

$$\bar{\phi} = \iint \phi(f, \chi_{st}) p(f, \chi_{st}) df d\chi_{st} \qquad (3.21)$$

Here ϕ refers to species mass fraction or temperature, the two parameters of key interest. The variables f and χ_{st} are assumed to be statistically independent so that the probability density function $p(f, \chi_{st})$ can be simplified as the product of the two individual PDFs, $p(f)$ and $p(\chi_{st})$ [Ferreira, 2001]. Accordingly, the probability of mixture fraction $p(f)$ obeys the β -function and is given as

$$p(f) = \frac{f^{\alpha-1}(1 - f^{\beta-1})}{\int f^{\alpha-1}(1 - f)^{\beta-1} df} \qquad (3.22)$$

where

$$\alpha = \bar{f}\left[\frac{\bar{f}(1-\bar{f})}{\bar{f}'^2} - 1\right] \qquad (3.23)$$

and

24

$$\beta = \left(1 - \overline{f}\right)\left[\frac{\overline{f}\left(1 - \overline{f}\right)}{\overline{f'^2}} - 1\right]$$

(3.24)

With the help of the aforementioned concept, mixture fraction can be utilized to describe the mixing process, and chemical reaction can be relaxed into a scalar dissipation rate. Moreover, chemistry and flow dynamics can be uncoupled into two PDFs. Consequently, the laminar flamelet model can assume one-dimensional behavior in the direction normal to the flame front. The local flame structure (or flamelet) can be described with only a few variables which combine the effect of complex chemical processes without the need to solve a transport equation for each chemical species of interest [Claramunt et al., 2004].

In this work, a standard k-ε two-equation model is exploited to simulate the turbulent effect. The mean mixture fraction $\overline{f}$ and its variance $\overline{f'}$ are solved via the following transport equations:

$$\frac{\partial}{\partial t}(\rho \overline{f}) + \nabla\left(\rho \overline{u} \overline{f}\right) = \nabla\left(\frac{\mu_t}{\sigma_t} \nabla \overline{f}\right)$$

(3.25)

$$\frac{\partial}{\partial t}(\rho \overline{f'^2}) + \nabla\left(\rho \overline{u} \overline{f'^2}\right) = \nabla\left(\frac{\mu_t}{\sigma_t} \nabla \overline{f'^2}\right) + C_g \mu_t \left(\nabla \overline{f}\right)^2 - C_d \rho \frac{\varepsilon}{k} \overline{f'^2}$$

(3.26)

where the default values for the constants σ_t, μ_t, C_g and C_d are 0.85, 2.86, and 2.0, respectively [Jones and Whitelaw, 1982]. The detailed information on the standard k-ε model is provided in Section 3.1.2.

3.2.4 Look-up Table Construction

According to Equation (3.21), the mean temperature and species fraction are only functions of mixture fraction f, its variance $\overline{f'^2}$ and the scalar dissipation rate at the position where f is stoichiometric χ_{st}. To reduce calculation time, FLUENT calculates the density-weighted mean species mass fractions and temperature once (Equation (3.18)). These results are then stored in a look-up table (see Figure 3.4) for subsequent usage in the simulation. There is one look-up table of this type for each scalar (such as temperature, species mass fraction) of interest. These look-up tables will change with variable χ_{st}. For certain χ_{st}, given the f and $\overline{f'^2}$ at a point in the flow domain, the mean values of mass fractions and temperature at that point can be obtained by interpolating the tabulated values.
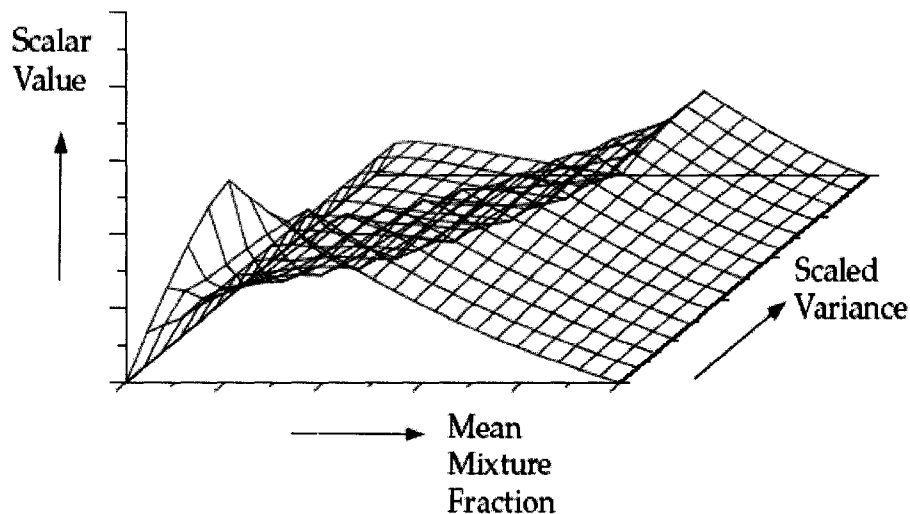
Fig. 3.4 Visual representation of a look-up table.

3.3 Flowchart of modeling

Figure 3.5 shows a flowchart, which presents the pre-processing stage and the simulating stage in FLUENT. The pre-processing stage is to calculate the mean species mass fractions and temperature and put them in a library. Those species mass fractions and temperature are functions of mixture fraction f, its variance $\overline{f'^2}$ and the scalar dissipation rate at stoichiometric (χ_{st}), which is preset. In the simulating stage, a k-ε turbulent model is adopted and the fluid flow is simulated to gain the localized mixture fraction and its variance. Product of species and temperature then can be obtained from the library in the pre-processing stage by using those localized known mixture fractions and variances in the simulating stage. As shown in Figure 3.5, the procedure of the pre-processing stage is from step 1 to step 5, while the simulating stage is in step 6.

The species and temperature are solved by two transport equations in the physical space.

$$\frac{\partial(\rho Y_i)}{\partial t} + div(\rho Y_i \vec{u}) = div\left(\rho D \nabla Y_i\right) + \dot{\omega}_i$$

$$\frac{\partial \rho h}{\partial t} + div(\rho \vec{u} h) = div\left(\rho D \nabla T\right) + \frac{\partial p}{\partial t}$$

①

The transport equations in the physical space are converted to ones in the **mixture fraction** space:

$$\rho \frac{\partial(Y_i)}{\partial t} = \rho \frac{\chi}{2 Le_i}\left(\frac{\partial^2 Y_i}{\partial f^2}\right) + \dot{\omega}_i$$

$$\rho \frac{\partial T}{\partial t} + \sum_{i=1} h_i \dot{\omega}_i = \rho \frac{\chi}{2}\frac{\partial^2 T}{\partial f^2} + \frac{1}{c_p}\frac{\partial p}{\partial t}$$

②

$\phi(f, \chi)$: local and instantaneous scalar quantities of interest like species fractions, density, temperature are function of **mixture fraction** f and **scalar dissipation rate** χ.

③   ④

In this work, the scalar dissipation rate is set to be $\chi = \chi_{st}$, because most of the chemistry occurs near $f = f_{st}$
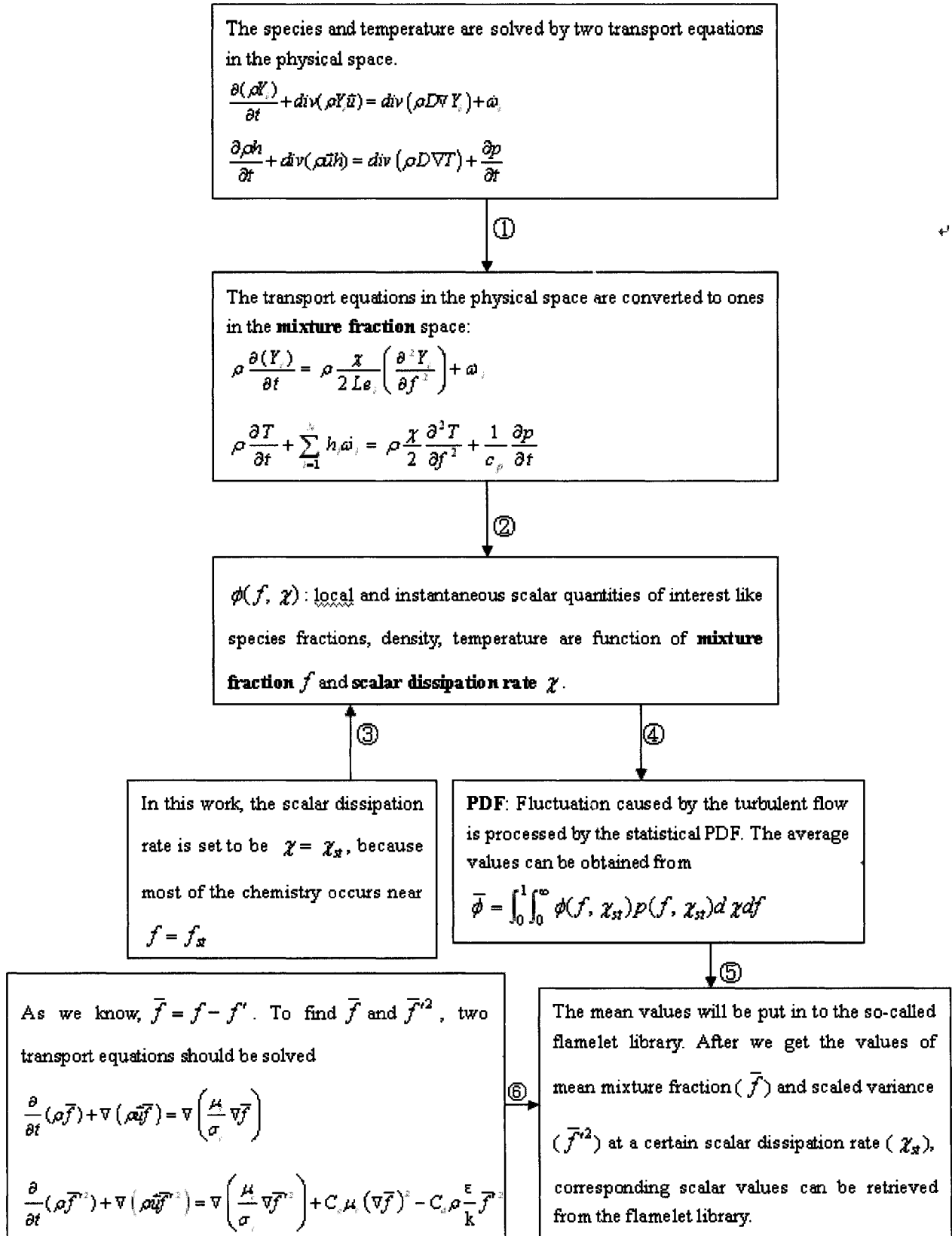
PDF: Fluctuation caused by the turbulent flow is processed by the statistical PDF. The average values can be obtained from

$$\bar{\phi} = \int_0^1\int_0^\infty \phi(f, \chi_{st}) p(f, \chi_{st}) d\chi df$$

⑤

As we know, $\bar{f} = f - f'$. To find $\bar{f}$ and $\bar{f'^2}$, two transport equations should be solved

$$\frac{\partial}{\partial t}(\rho \bar{f}) + \nabla\left(\rho \vec{u} \bar{f}\right) = \nabla\left(\frac{\mu}{\sigma}\nabla \bar{f}\right)$$

$$\frac{\partial}{\partial t}(\rho \bar{f'^2}) + \nabla\left(\rho \vec{u} \bar{f'^2}\right) = \nabla\left(\frac{\mu}{\sigma}\nabla \bar{f'^2}\right) + C_g \mu \left(\nabla \bar{f}\right)^2 - C_d \rho \frac{\varepsilon}{k}\bar{f'^2}$$

⑥

The mean values will be put in to the so-called flamelet library. After we get the values of mean mixture fraction ($\bar{f}$) and scaled variance ($\bar{f'^2}$) at a certain scalar dissipation rate (χ_{st}), corresponding scalar values can be retrieved from the flamelet library.

Fig. 3.5 Flowchart of the modeling calculation.

3.4 Flow Configuration of Masri-Bilger Flame

Recently, theoretical study focuses on numerical simulation of turbulent diffusion combustion. Meanwhile, reliable and well-documented experimental flames are needed to verify those models used for numerical simulation. To do an experiment of a burner, the measurements should include turbulence, chemical kinetics, thermal radiation and pollutant formation, etc. Many burner geometries for turbulent nonpremixed flames have been investigated, including the unpiloted jet burner [Hawthorne et al., 1949], the pilot stabilized jet burner, the bluff-body burner [Dally et al., 1998] and the swirling jet burner [Pillipp et al., 1992], which is in the order of complexity.

The thermofluids research group at the University of Sydney provides many detailed data archives. The piloted turbulent methane/air jet flames are used in this work, which is very convenient to study the effects of the interaction between turbulence and chemistry in flames. The details of the experimental measurement setup for the Masri-Bilger pilot jet flame are presented in Appendix A. The simplicity of the flow and the existence of a fully turbulent region of the flame where the chemical kinetic effects are significant make this burner an ideal test case for testing and development of computer models

ANSYS FLUENT is the state-of-the-art computational fluid dynamics software. Based on the finite volume method, the software can simulate fluid flow and heat transfer in complex geometries. In this work, to solve the transport equations, the velocity-pressure

29

complex geometries. In this work, to solve the transport equations, the velocity-pressure

coupling is processed by Semi-Implicit Method for Pressure-Linked Equations (SIMPLE

algorithm). The algorithm was put forward by Patankar [1980]. Specifically, the first

order upwind scheme is utilized in the discretization of the transport equations.

The well known Masri-Bilger [University of Sydney, 1984] piloted methane/air jet flame

is used as the benchmark in this study. It consists of a fuel jet (100% CH_4), an annular

pilot jet of hot gases, which are premixed flames with a stoichiometric mixture fraction

for flame stabilization, and surrounded by a co-flow of air (shown in Figures 3.5 and 3.6).

The diameter of the fuel jet is 7.2mm; the one for the pilot jet is 18mm and for the
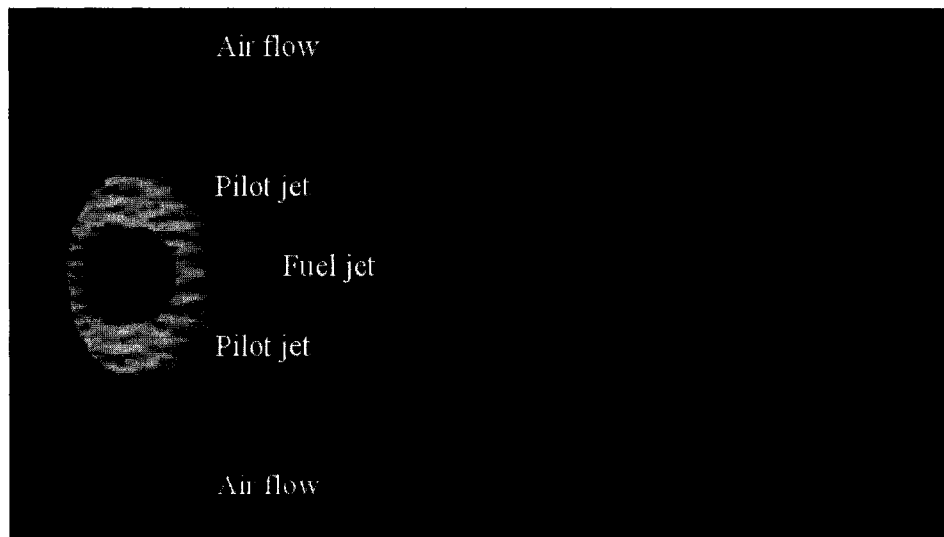
co-flow air is 288mm.

Fig. 3.6 The Masri-Bilger piloted methane/air jet flame [University of Sydney, 1984].

In this study, we only consider the case where the pilot jet velocity is 24m/s, the air velocity is 15m/s, and the fuel jet velocity is 41m/s. Figure 3.7 shows the calculation domain with 13740 cells, 27813 faces and 14074 nodes. For the purpose of reducing calculation time and increase the accuracy, the distribution of mesh is arranged exponentially. This is done by overlaying the solution domain and let most of the nodes concentrate near the stoichiometric locations. The mesh details including sensitivity analysis is provided in Appendix B.
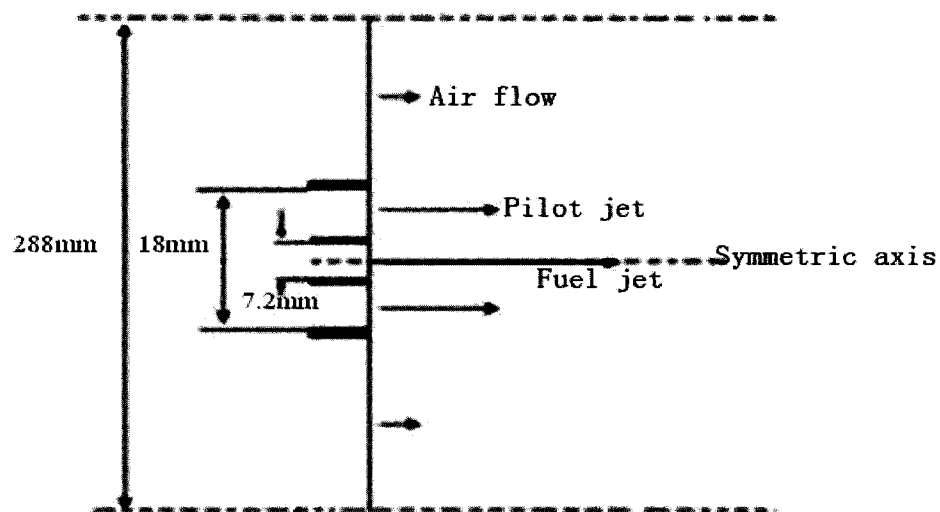

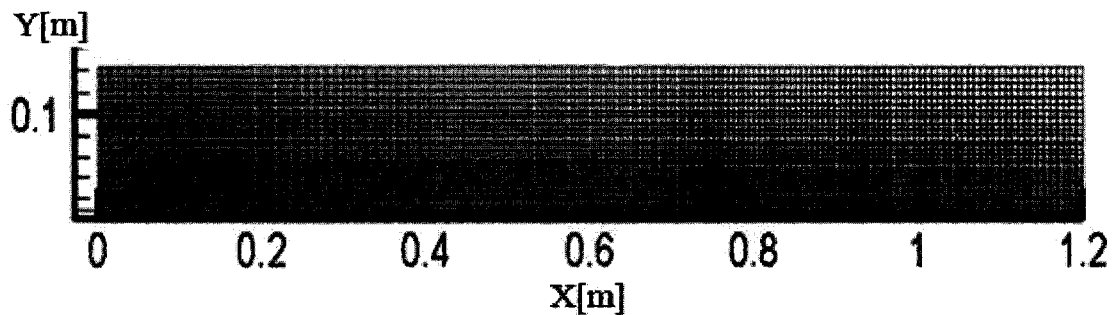Fig. 3.7 Geometrical configuration of the Masri-Bilger piloted jet flame.

Fig 3.8 Mesh for the calculation domain.

boundary along the x-axis is set as 'axis', that is, nothing crosses this line. Since the

details of the flow velocity and pressure are not known at the flow exits, outlet 1 and

outlet 2 are set as 'outflow' as shown in Figure 3.8. This 'outflow' is handled in

FLUENT by using an extrapolation procedure to update the outflow velocity and pressure,

without influencing the flow upstream. The calculations are assumed to converge when

the residuals of continuity, x-velocity, y-velocity, mean mixture fraction and mixture
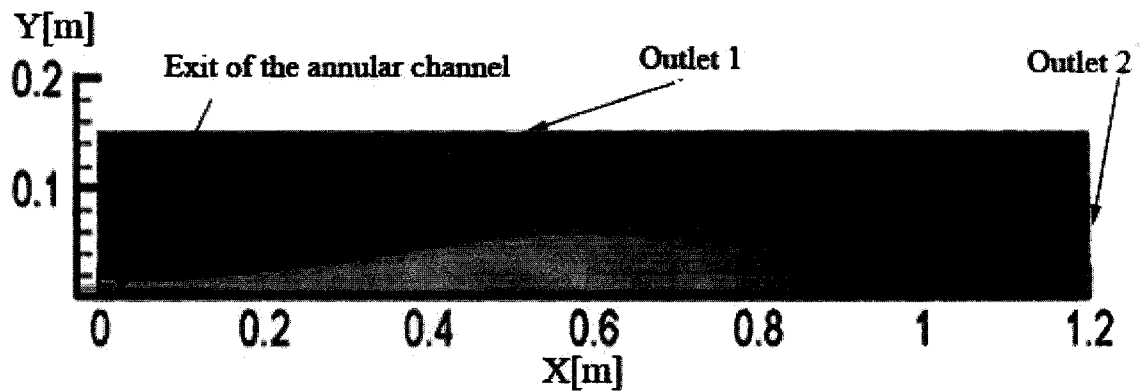
fraction variance are less than 1×10^{-4}.

Fig. 3.9 Flame in the calculation domain.

CHAPTER 4

RESULTS AND DISCUSSION

4.1 Skeletal Versus Detailed Chemical Reaction Mechanisms

Masri and Pope [1990] pointed out that the interaction of turbulence and chemistry is most pronounced between 20d and 30d (d is the diameter of the fuel jet) downstream of the base. Thus, we focus on the details at 20d and 30d, where data reduction is conducted. Specifically, the radial distributions of mean temperature and mean mass fractions of CH_4, CO_2 and CO calculated by FLUENT based on Smooke's Skeletal (Appendix C) and GRI-Mech 3.0 mechanisms are compared with the experiment. The experimental data are from University of Sydney in 1984. A total of 1250 data points have been taken at each location in the flame. The uncertainties are estimated based on the standard deviation of the measured data and shown as error bars on the subsequent figures.

4.1.1 Flamelet Libraries Analysis

As mentioned at the end of Chapter 3, laminar flamelet modeling has a preprocessing step to calculate the species of interest and temperature by solving the density-weighted mean species mass fractions and temperature equations (Equation (3.18)) and the numerical results are stored in the flamelet libraries. Figure 4.1 shows the temperature contour of the Masri-Bilger piloted jet flame with the Skeletal mechanism, from which we can see

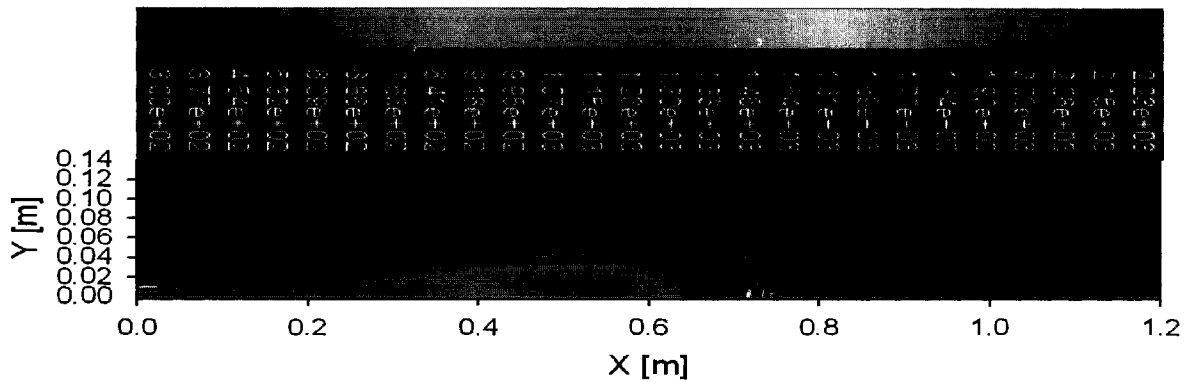that the maximum temperature of the flame is about 2230K.

Fig 4.1 Contour of temperature [K] of the pilot jet flame.

More detail could be obtained from the flamelet libraries. When we inspect the temperature and the amount of species corresponding to mean mixture fraction, the following figures (Figures 4.2-4.4) show that no detectable difference is made between the model with Skeletal mechanism and that with a detailed GRI-Mech 3.0 mechanism. Figure 4.2 shows that the maximum mean temperature is 2237K and it occurs at mean mixture fraction 0.0582. It indicates that the heat is mainly produced at the stoichiometric location, which corresponds to a mixture fraction of 0.055. This is because of the main chemical reaction at these locations. On the pure air side and the pure fuel side when the mean mixture fractions equal to zero and one, they all get 300K, which means no reaction occurs at those places.
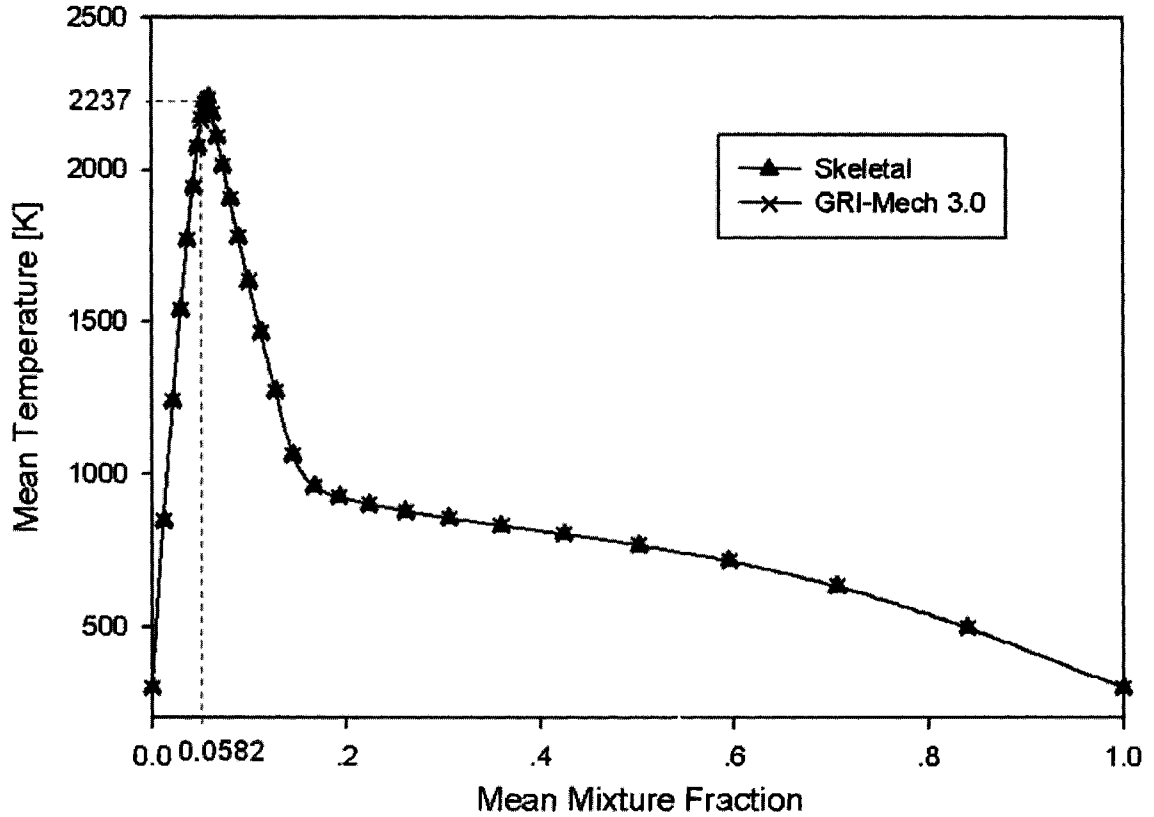
Fig 4.2 Mean temperature distribution changing with mean mixture fraction.

Figure 4.3 shows mass of fraction of CO_2 changing with mean mixture fraction. The

maximum of mass fraction of CO_2 is 0.08594 and occurs at the location when mean

mixture fraction equals to 0.0547. This is very close to the stoichiometric value 0.055

and nearly at the same location where the highest temperature occurs, which indicates that

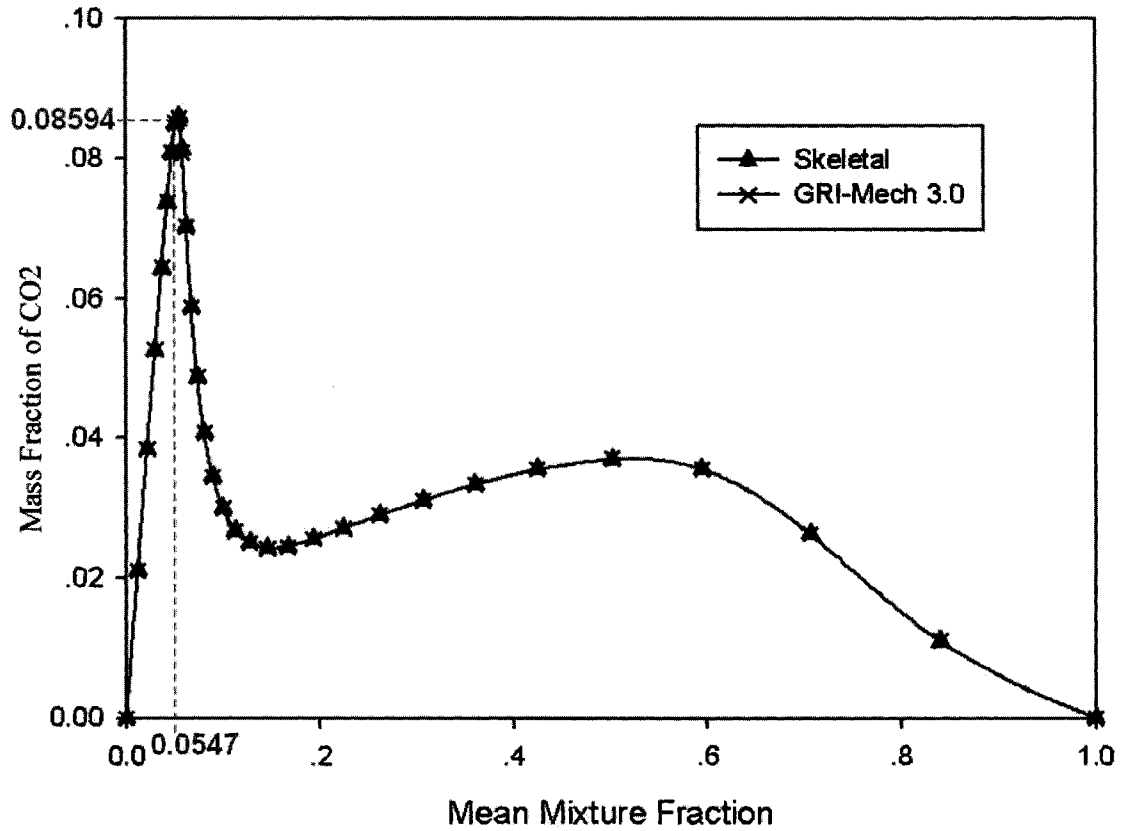combustion of fuel and oxidizer at stoichiometry would lead to maximum generation of

CO_2.

Fig 4.3 Mass fraction of CO_2 changing with mean mixture fraction.

Figure 4.4 shows the mass fraction of CO changing with the mean mixture fraction. It can be seen that the maximum of mole fraction occurs at the location when the mean mixture fraction equals to 0.167, which indicates incomplete combustion mostly takes place there.
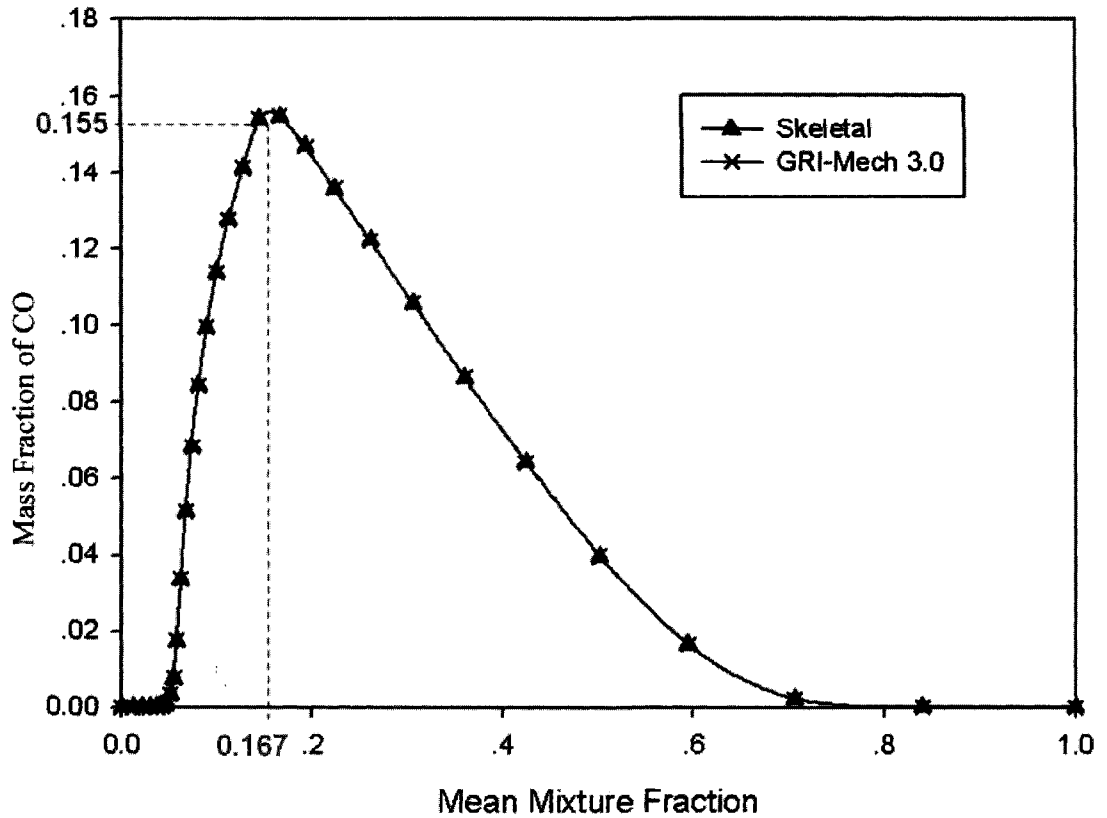
Fig 4.4 Mass fraction of CO changing with mean mixture fraction.

4.1.2 Results of Skeletal Versus Detailed Chemical Reaction Mechanisms

We can see from Figure 4.5 (where r is the radial distance from the center and R_0 is the radius of the fuel jet inlet) that the detailed mechanism is only marginally better in predicting the radial distributions of CH_4 at 20d and 30d. In other words, the skeletal mechanism is adequate as far as CH_4 prediction is concern.
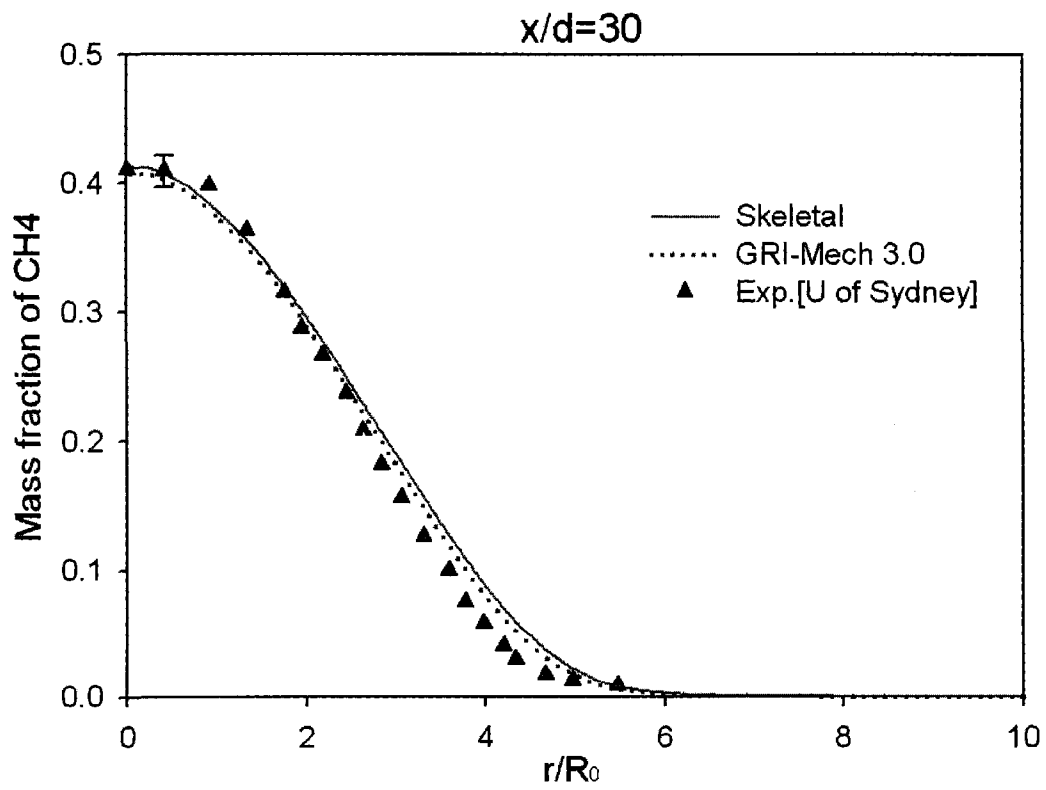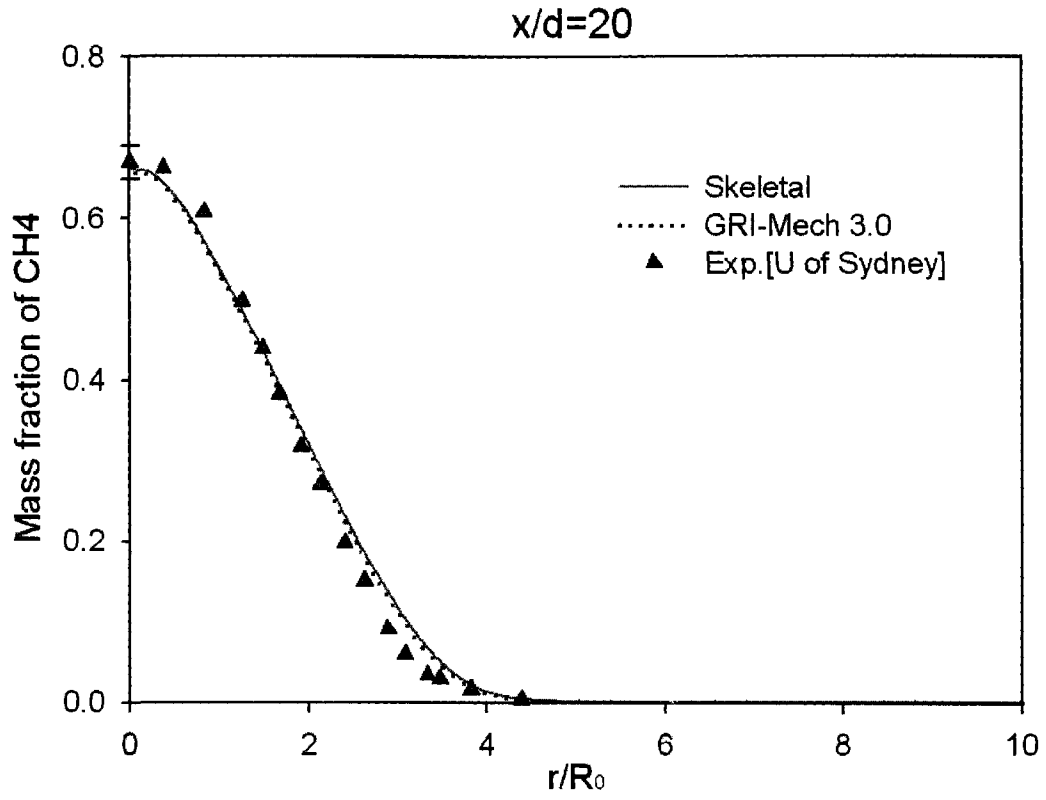
Fig. 4.5 Mass fraction of CH_4 at 20d and 30d.

The temperature profiles are plotted in Figure 4.6. It is clear that both mechanisms lead to approximately the same temperature distribution. At 20d, the predicted temperatures agree reasonably well with measurement at the center of the jet and also near the edge of the flame. The models, however, over-predict the maximum temperature by around 200K at r/R_0 of approximately 3.0. This temperature over-prediction worsens significantly farther downstream. At 30d downstream, the predicted temperature is over 100K higher than the experimental value at the center of the jet, and the peak temperature is over-predicted by more than 400K. The largest discrepancy appears to occur around the region where rigorous combustion is expected to take place. Any incomplete combustion in this region can result in significant drop in the flame temperature. The greater deviation at axial location 30d than that at 20d is probably caused by the progress of the extinction phenomenon with axial distance. Neglecting heat losses may have also contributed to the temperature over-prediction.
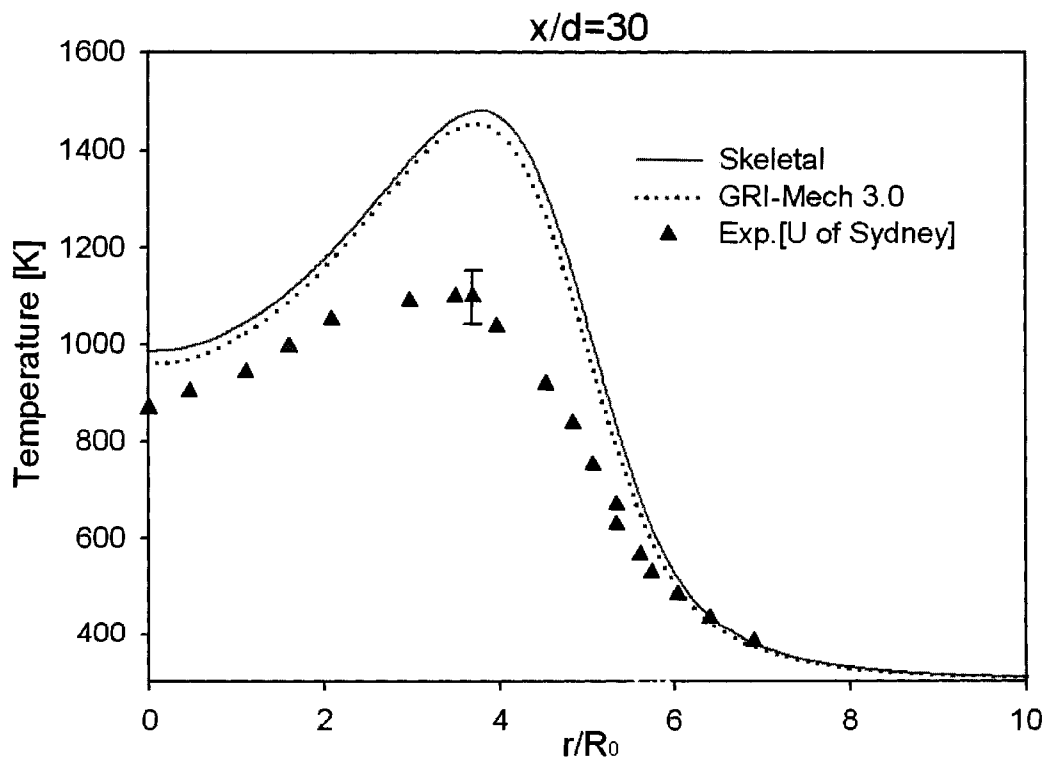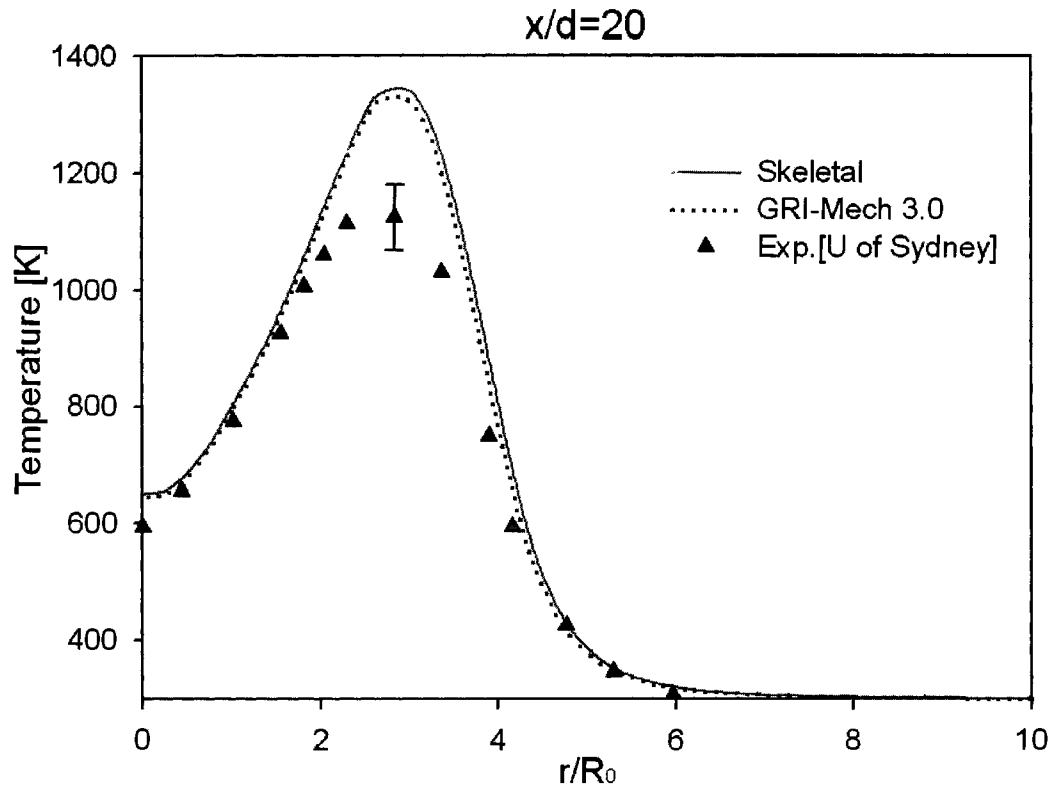
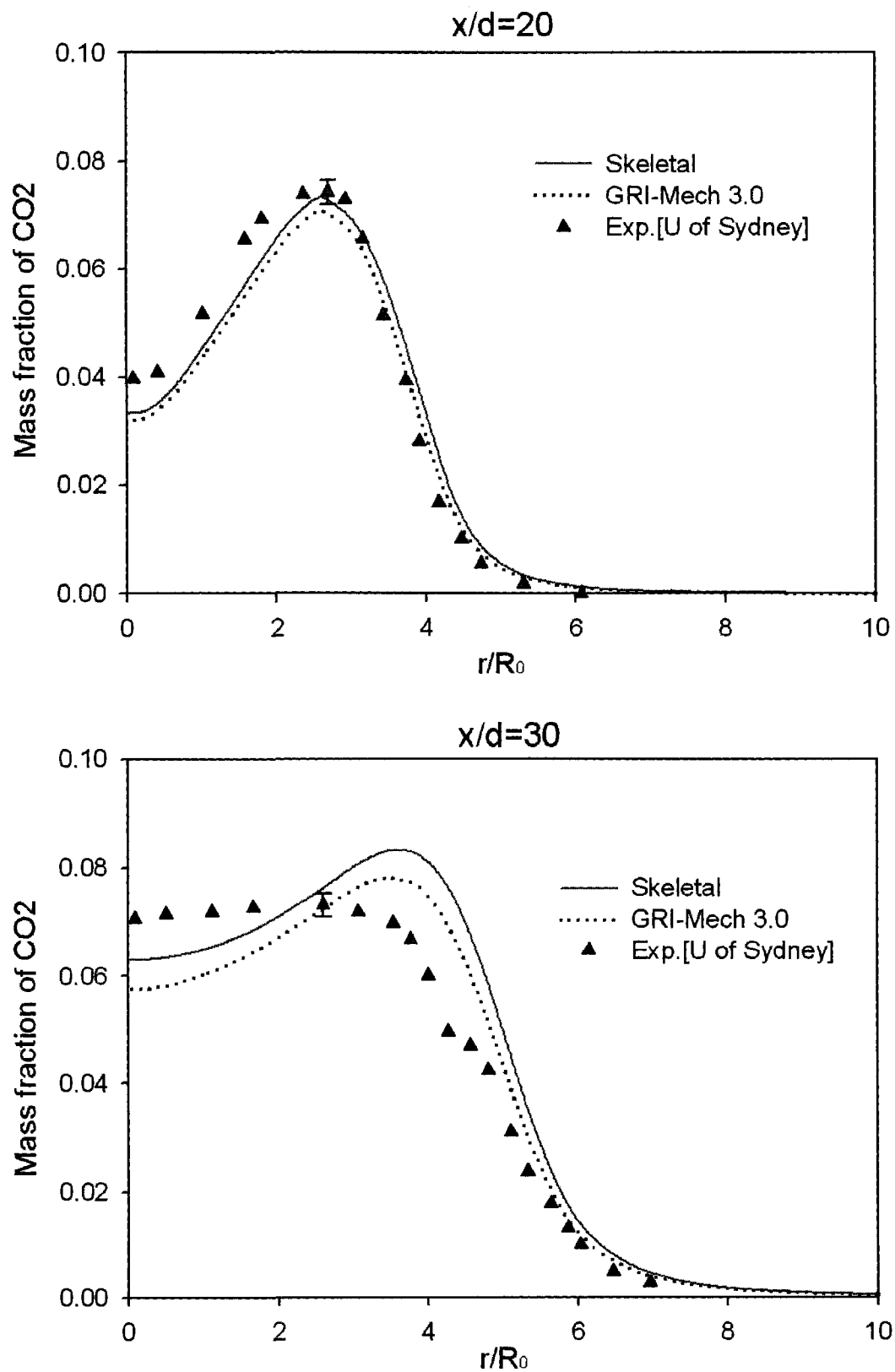Fig. 4.6 Mean radial temperature at 20d and 30d.

Fig. 4.7 Mass fraction of CO_2 at 20d and 30d.

Figure 4.7 shows the CO_2 mass fraction distribution. Around the center of the jet, the skeletal mechanism seems to lead to better agreement with the experiment. Overall, however, the detailed GRI mechanism predicts the CO_2 distribution better. We see that even though both models appear to predict the fuel consumption correctly (Figure 4.5), neither model could capture the CO_2 formation accurately. Both models underestimate CO_2 concentration around the jet core and overestimate the peak value at 30d. The overestimation of CO_2 appears to correspond to the over-prediction in the peak temperature (Figure 4.6), resulting in larger than expected peak CO_2 prediction. The reason behind the somewhat underestimation of CO_2 around the core at 30d is not clear.

It is clear from Figure 4.8 that the detailed GRI mechanism leads to marginally better CO estimation. More importantly, Figure 4.8 depicts that neither the skeletal nor the detailed mechanism, when utilized within the assumptions imposed by our model in FLUENT, can predict the CO concentration accurately. The higher than predicted CO appears to indicate the occurrence of significant amount of incomplete combustion around the core of Masri-Bilger jet flame.

Compared to the flamelet libraries, it is found that the maximum production of CO is way lower, which indicate that incomplete reaction is not very pronounced in the location x/d=20, and x/d=30.
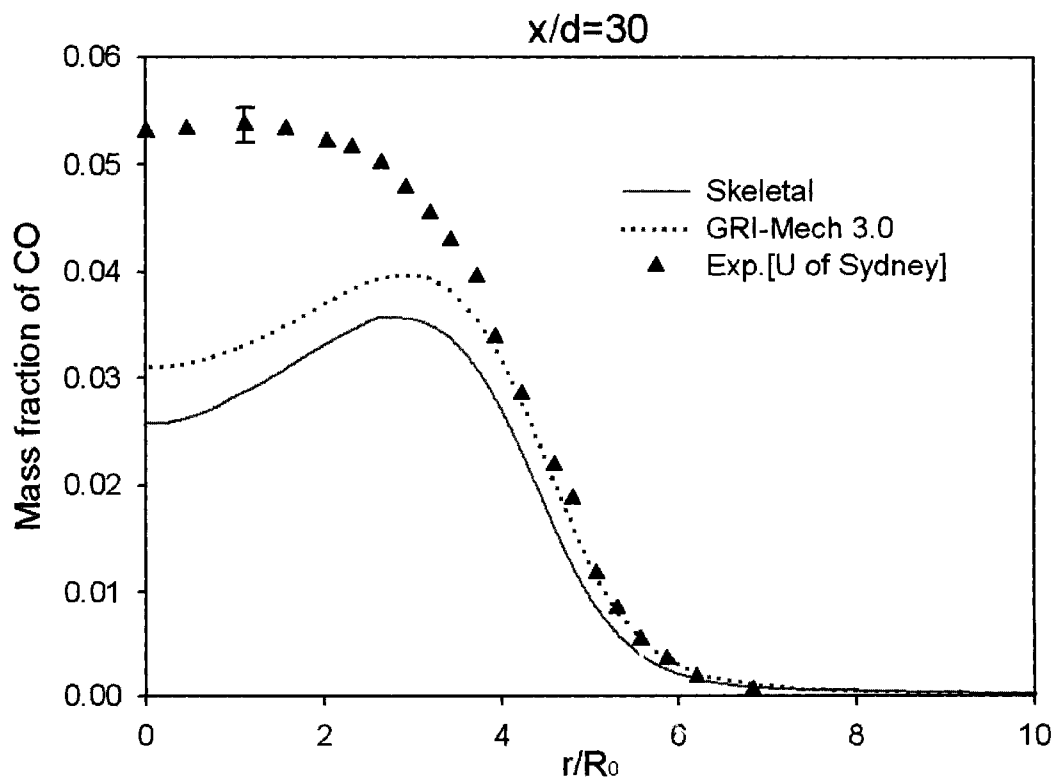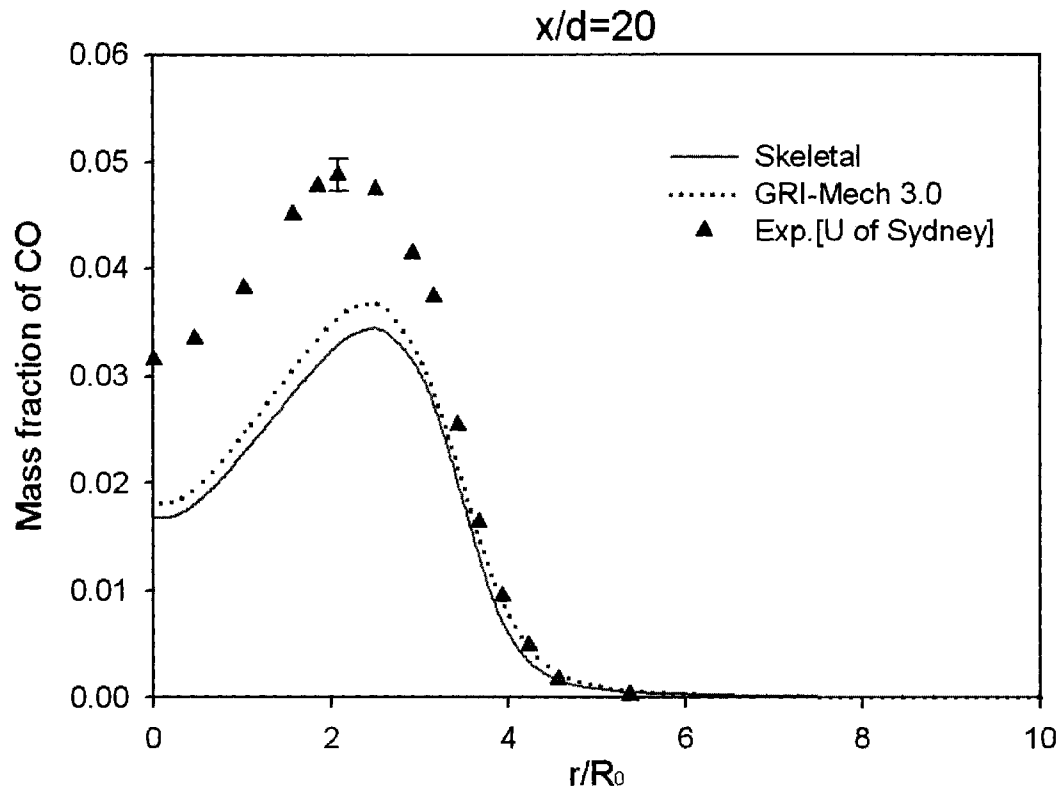
Fig. 4.8 Mass fraction of CO at 20d and 30d.

4.2 Variable Scalar Dissipation Rates

The above section shows that only small difference is made to radial distribution of the species (CO_2 & CO) and the temperature by using the steady laminar flamelet model with the detailed GRI mechanism and the skeletal mechanism. To reduce the computation time, the skeletal mechanism is utilized for studying the effect of scalar dissipation rate. Data reduction is conducted at the axial location x=30d, where the interaction of turbulence and chemistry is relatively strong. The scalar dissipation rate is varied from 0.001 s^{-1} (close to equilibrium), to 10 s^{-1}, and subsequently to 20 s^{-1}.

Fig. 4.9 Radial distribution of mass fraction of CH_4 at x/d=30 under different scalar dissipation rates.

Figure 4.9 shows the radial distribution of mass fraction of CH_4 under different scalar dissipation rates. We see that irrespective of the scalar dissipation rate, the predicted CH_4 concentrations agree well with the experiment.

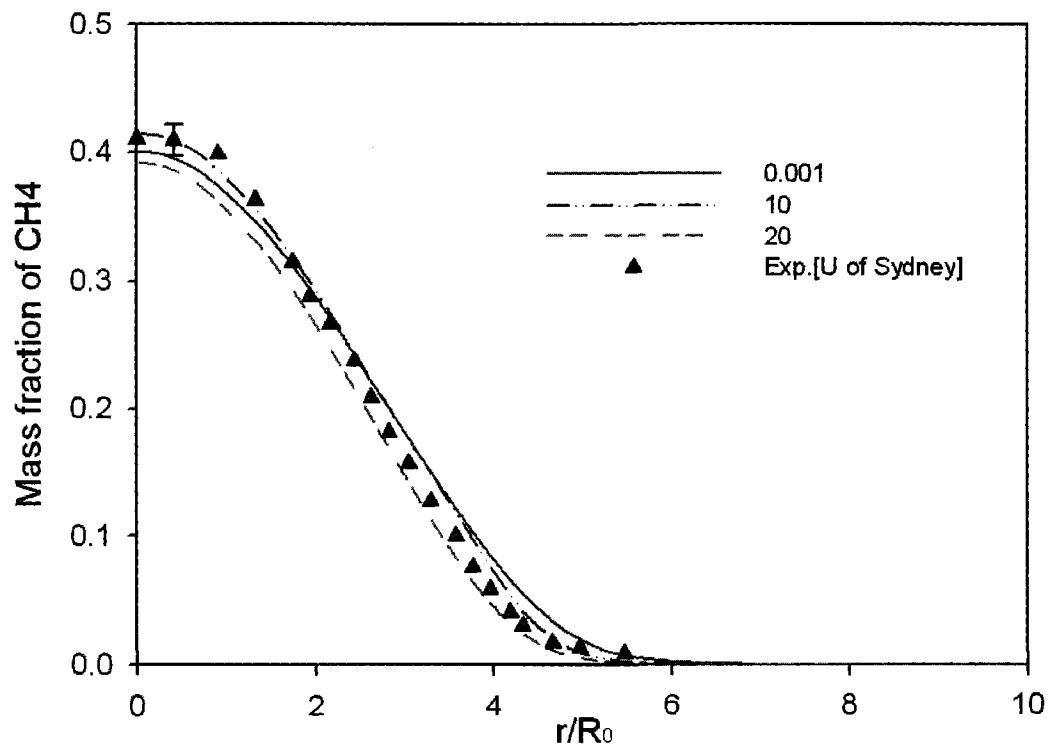Figure 4.10 shows the radial distribution of mean temperature under different scalar dissipation rates. The increase in the value of the scalar dissipate rate significantly improve the temperature prediction. In other words, the equilibrium (no slowing down of local combustion rate) assumption over-predicts the combustion rate and hence, the resulting combustion temperature. A scalar dissipation rate of 20 s^{-1} seems to be the maximum that can be meaningfully applied, without under-predicting the temperature near the core of the jet and also the region far away.

Figure 4.11 shows the radial distribution of mass fraction of the pollutant CO_2 under the influence of different scalar dissipation rate. Overall, the model with the highest scalar dissipation rate appears to better predict the CO_2 concentration. The somewhat under prediction around r/R_0 of 5 to 6 seems to indicate that a scalar dissipation rate of 20 s^{-1} is probably the upper limit.
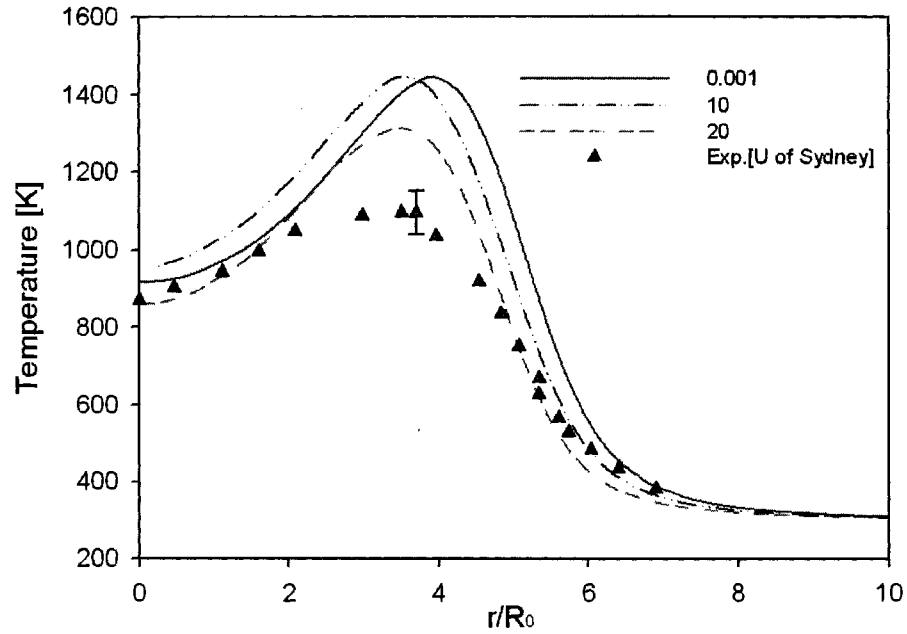
Fig. 4.10 Radial distribution of mean temperature at x/d=30 under different scalar
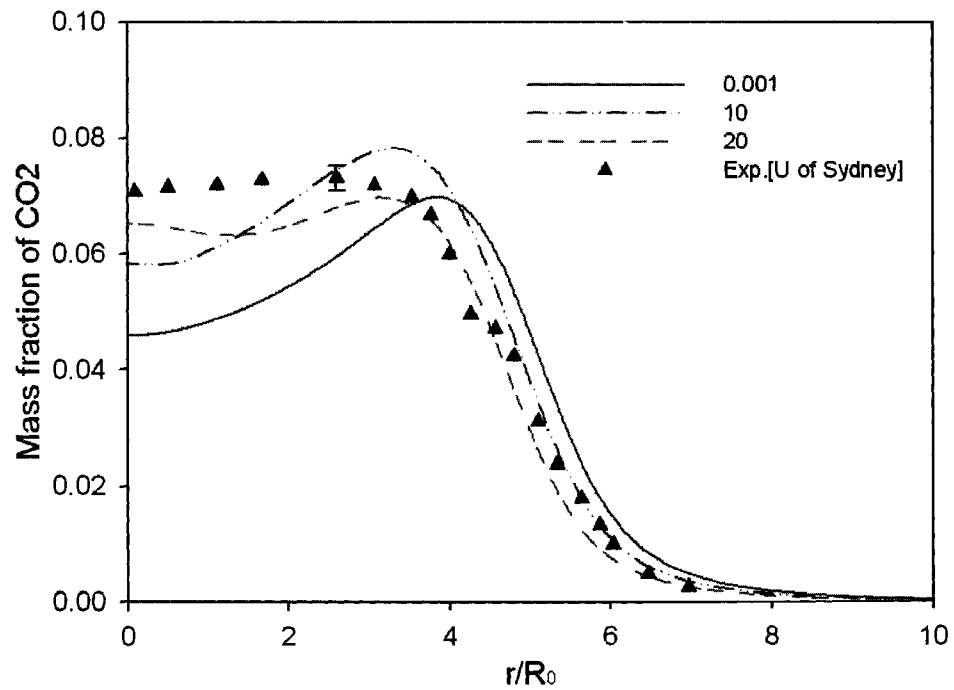
dissipation rates.

Fig.4.11 Radial distribution of mass fraction of CO_2 at x/d=30 under different scalar

dissipation rates.

Figure 4.12 shows the radial distribution of mass fraction of CO under the effect of different scalar dissipation rates. The fast chemistry with 0.001 s^{-1} dissipation rate over-predicts the CO concentration from the core to the radial location where no more CO is produced. Assuming a scalar dissipation rate of 10 s^{-1} appears to lead to the best results.
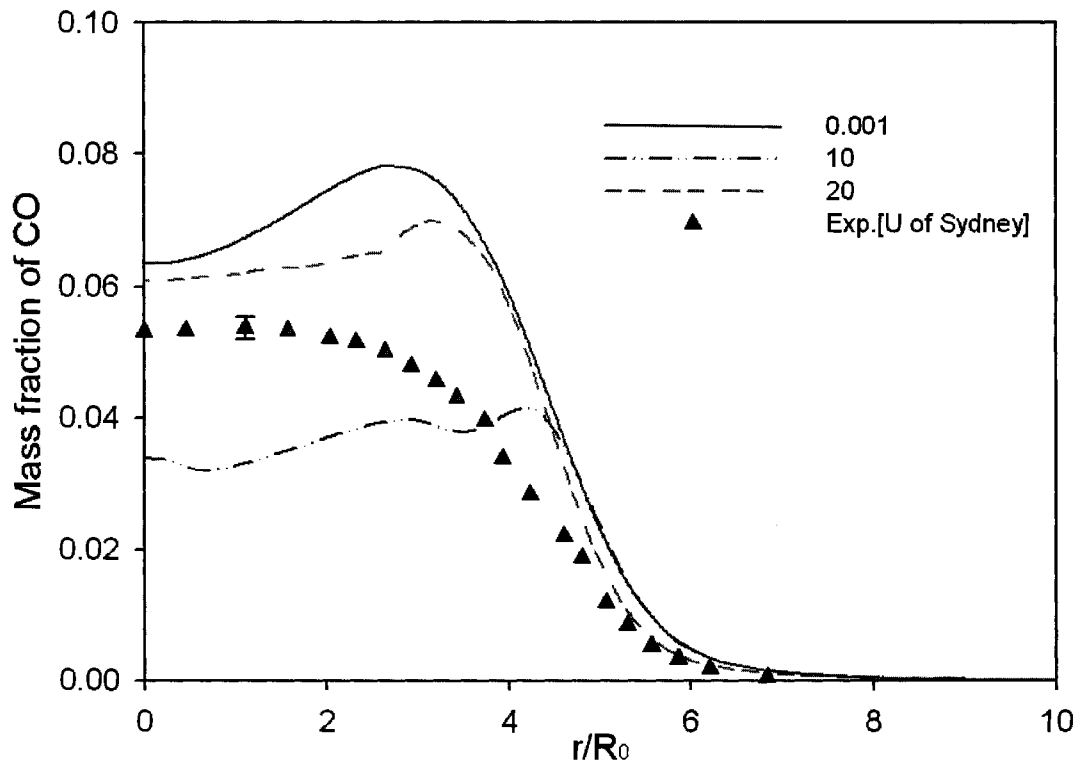

Fig. 4.12 Radial distribution of mass fraction of CO at x/d=30 under different scalar dissipation rates.

The present models predict unrealistic low concentrations of nitric oxide (NO), a pollutant of major concern. The main reason is that the steady laminar flamelet model

adopts fast chemistry and hence, there is not enough time for the slowing forming species

such as NO to accumulate.

CHAPTER 5

CONCLUDING REMARKS AND RECOMMENDATIONS

5.1 Conclusions

In this thesis, the steady laminar flamelet concept is discussed. Through the introduction of the mixture fraction co-ordinate system and the concept of PDF, complicated combustion phenomenon can be described by only three variables, which are the mean mixture fraction ($\bar{f}$), the mixture fraction variance ($\bar{f'^2}$) and the scalar dissipation rate at the stoichiometric mixture fraction f_{st} (χ_{st}).

The effect of reaction mechanism has been briefly evaluated within the steady laminar flamelet framework. It is found that within the assumptions imposed in this study, the detailed GRI mechanism is only marginally better than Smooke's [1991] skeletal mechanism. While the qualitative fuel, temperature, CO_2 and CO trends are more or less captured, both mechanisms when utilized within the steady laminar flamelet model failed to accurately predict the temperature and CO concentration, in particular.

The model near equilibrium (0.001 s^{-1}) is not suitable for simulating the nonpremixed combustion phenomenon caused by extinction and reignition. However, by increasing the scalar dissipation rate up to $20\,s^{-1}$, a better agreement of the model with the experiment can be gained.

5.2 Recommendations for Future Works

For turbulent combustion, the complication of chemical reactions and chemical kinetics, randomicity of the turbulence phenomenon and intricate interaction of turbulence and chemistry are partially solved. With the increasing capacity of computational equipments, improvements to this model can be expected, which are summarized here.

Firstly, from the above conclusion, we know that the steady-state assumption cannot accurately describe the whole domain of the nonpremixed combustion since turbulent flows are usually in a highly non-homogeneous and unsteady status, which lead to rapidly changing scalar dissipation rate. This work also indicates that the laminar flamelet structure can not respond to the rapid changes of scalar dissipation rate instantaneously. The model can be improved by considering the response delay and a transient laminar flamelet model can be used to describe flamelet structures by introducing a relevant time variable to describe the flamelet structures.

Secondly, the k-ε two equation model is widely used to simulate the turbulent effect of the reacting fluid flow. The Reynolds Stress Model (RSM), however, has been developed for the last 20 years and is considered as a higher level, elaborate turbulence model. Modeling results can be improved by coupling RSM to the SLFM. Also, by coupling RSM to the transient laminar flamelet model, better results can be expected.

Work is in progress to extend this study to include the extinction phenomenon. The

unity Lewis number assumption can also be relaxed, and so can the adiabatic assumption.

REFERENCES

Bilger, R.W., "Turbulent flows with nonpremixed reactants," Turbulent Reacting Flows, Libby, P. A. and William, F. A. (eds.), Springer-Verlag, pp. 65-113, 1980.

Bilger, R.W., "The structure of turbulent nonpremixed flames," 22nd Symposium (International) on Combustion, the Combustion Institute, pp. 475-488, 1988.

Bilger, R.W., "Conditional moment closure for turbulent reacting flow," Physics of Fluids, Vol. 5, pp. 436-444, 1993.

Bray, K.N. and Peters, N., Turbulent Reacting Flows, P.A. Libby & F.A. William (eds.), Springer-Verlag, Academic Press, vol. 63, pp. 114-118, 1994.

Claramunt, K., Consul, R., Carbonell, D. and Perez-Segarra, C.D., "Laminar flamelet concept for laminar and turbulent diffusion flames," AIAA paper 2004-796.

Dally, B.B., Masri, A.R., Barlow, R.S. and Fiechtner, G.J., "Instantaneous and mean compositional structure of bluff-body stabilized nonpremixed flames," Combustion and Flame, Vol. 114, pp. 119-148, 1998.

Dibble, R.W., Masri, A.R. and Bilger, R.W., "The spontaneous Raman scattering technique applied to nonpremixed flames of methane," Combustion and Flame, Vol. 67, pp. 189-206, 1987.

Dixon-Lewis, G., "Structure of laminar flame," 23rd Symposium (International) on Combustion, the Combustion Institute, pp. 305-324, 1990.

Ferreira, J.C., "Steady and transient flamelet modeling of turbulent non-premixed

combustion," Progress in Computational Fluid Dynamics, Vol. 1, Nos. 1/2/3, 2001.

Ferziger, J.H. and Peric, M., Computational methods for fluid dynamics, Springer Verlag, pp. 257, 1999.

FLUNET 6.2 User's Guide, 2005.

Hawthorne, W.R., Weddell, D.S., and Hottel, H.C., "Mixing and combustion in turbulent jets," 3rd Symposium (International) on Combustion, the Combustion Institute, pp. 266-288, 1949.

IEA Countries 2001 review, International Energy Agency, http:// www.iea.org/index.html, accessed on June 1, 2008.

Jones, W.P. and Whitelaw, J.H., "Calculation methods for reacting turbulent flows: a review," Combustion and Flame, Vol. 48, pp. 1-26, 1982.

Launder, B.E. and Spalding D.B., "The numerical computation of turbulent flows," Computer Methods in Applied Mechanics and Engineering, Vol. 3, pp. 269-289, 1974.

Lesieur, M. and Metais, O., "New trends in large eddy simulations of turbulence," Annual Review of Fluid Mechanics, Vol. 28, pp. 45-82, 1996.

Masri A.R. and Pose S.B., "PDF calculations of piloted trubulent nonpremixed flames of methane," Combustion and Flame, Vol. 81, pp.13-29, 1990.

Patankar, S.V., Numerical Heat Transfer and Fluid Flow, Hemisphere Publishing Corp., pp. 210-237, 1980.

Peeters, T., "Numerical modeling of turbulence natural-gas diffusion flames," PhD Thesis, Delft Technical University, Delft, the Netherlands, 1995.

Peters, N., "Laminar diffusion flamelet models in non-premixed turbulent combustion," Progress in Energy and Combustion Science, Vol. 10, pp. 319-339, 1984.

Peters, N., "Laminar flamelet concepts in turbulent combustion," 21st Symposium (International) on Combustion, the Combustion Institute, pp. 1231-1250, 1986.

Peters, N., Turbulent Combustion, Cambridge University Press, 2000.

Philipp, M., Hofmann, S., Habisreuther, P., Lenze, B. and Eickhoff, H., "Experimental and numerical study concerning stabilization of strongly swirling premixed and nonpremixed flames," 24th Symposium (International) on Combustion, the Combustion Institute, pp. 361-368, 1992.

Pope, S.B., "PDF methods for turbulent reactive flows," Progress in Energy and Combustion Science, Vol. 11, pp. 119-192, 1985

Rogg, B., Behrendt, F. and Warnatz, J., "Modelling of turbulent methane-air diffusion flames: the laminar-flamelet model," Journal of Physical Chemistry, Vol. 90, pp. 1005-1010, 1986.

Sivathanu, Y.R. and Faeth, G.M., "Generalized state relationships for scalar properties in non-premixed hydrocarbon/air flames," Combustion and Flame, Vol. 82, pp. 211-230, 1990.

Skevis, G., Goussis, D.A. and Mastorakos, E., "Understanding methane flame kinetics from reduced mechanisms," International Journal of Althernative Propulsion, Vol. 1, pp. 216-227, 2007.

Smooke, M.D., Puri, I.K. and Seshadri, K., "A comparison between numerical

calculations and experimental measurements of the structure of a counterflow diffusion flame burning diluted methane in diluted air," 21st Symposium (International) on Combustion, the Combustion Institute, pp. 1783-1792, 1986.

Smooke, M.D., "Reduced kinetic mechanisms and asymptotic approximations for methane-air flames," Lecture Notes in Physics, Vol. 384, 1991.

Smith, G.P., Golden, D.M., Frenklach, M., Moriarty, N.W., Eiteneer, B., Goldenberg, M., Bowman, C.T., Hanson, R.K., Song, S., Gardiner, W.C., Jr., Lissianski, V.V., and Qin, Z., http://www.me.berkeley.edu/gri_mech, 2000, accessed on Feb 1st, 2008.

Swaminathan, N., " Flamelet regime in non-premixed combustion," Combustion and Flame, Vol. 129, pp. 217-219, 2002.

University of Sydney, Thermofluids research group, http://www.aeromech.usyd.edu.au/thermofluids/main_frame.htm, 1984.

Veynante, D. and Vervisch, L., "Turbulent combustion modeling," Progress in Energy and Combustion Science, Vol. 28, pp. 193-266, 2002.

APPENDICES

APPENDIX A

EXPERIMENTAL TEST SETUP

When conducting an experiment of turbulent flame combustion, we require measurement

techniques to acquire those data in which we are interested. For those data from the

University of Sydney that are used to compared with the model of this work, a Raman
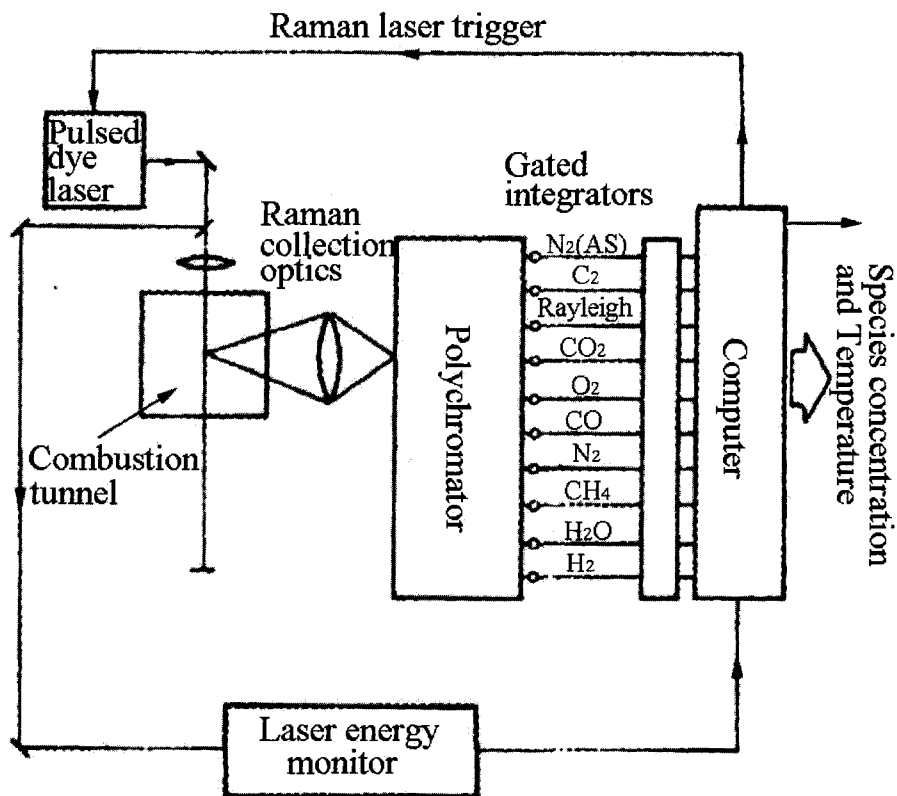
scattering technique was adopted.

Fig. A.1 Schematic of the experimental test setup of the Masri-Bilger pilot jet flame

[Dibble, et al., 1987].

Figure B.1 shows the experimental test setup for the Masri-Bilger pilot jet flame [Dibble, et al., 1987]. The details of the combustion tunnel are shown in Figure B.2. The test section and contraction cone were mounted on a traversing mechanism driven by stepping motors to provide positioning in three orthogonal directions. The advantage of the spontaneous Raman scattering technique is its capability of providing instantaneous, spatially resolved measurements of temperature and all the major species simultaneously using only a single laser beam without tuning.
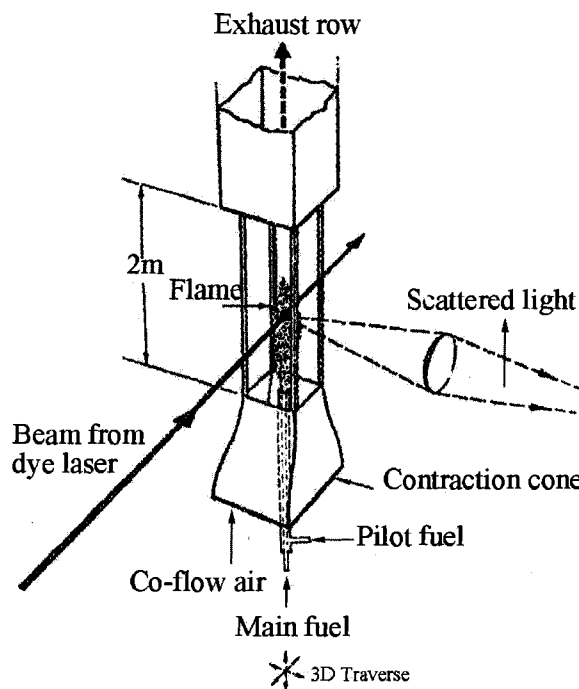

Fig. A.2 Schematic of the combustion tunnel for the Masri-Bilger pilot jet flame [Dibble, et al., 1987].

APPENDIX B

SENSITIVITY ANALYSIS

The computational domain is made by the commercial software GAMBIT. GAMBIT put mesh nodes along the edge such that the ratio of any two succeeding interval lengths is constant, which is given,

$$R = \frac{l_{i+1}}{l_i} \tag{B.1}$$

where l_i and l_{i+1} are the lengths of intervals i and $i+1$, respectively, and R is the constant interval length ratio as shown in Figure B.1. This valve can be determined by different types of edge mesh grading schemes, including Successive ratio, First length, Fast length, First last ratio, Last first ratio, Exponent, Bi-exponent and Bell shaped.
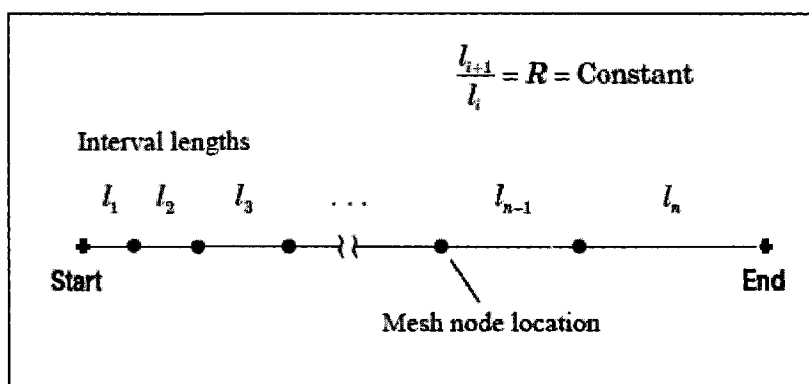

Fig B.1 Edge mesh grading parameters

In this work, to resolve the fine structure of the inner zone where most of the reaction

takes place, the exponent scheme is adopted. For this scheme, the interval length ratio R is written as

$$R = e^{(L/n)(x-1/2)}$$ (B.2)

where L is edge length, n presents number of intervals and x signifies a user-specified input parameter.

Table B.1 shows the time of convergence under different x. The sensitivity of the model using different R for the calculation domain is plotted in Figure B.1. The results do not converge when x is equal to 0.5 (R=1). Although no big difference is made among x=0.3, x=0.35 and x=0.4, the parameter x=0.35 obtains best accuracy and reduces the calculation time.

Table B.1 Time of convergence corresponding to different value of parameter x

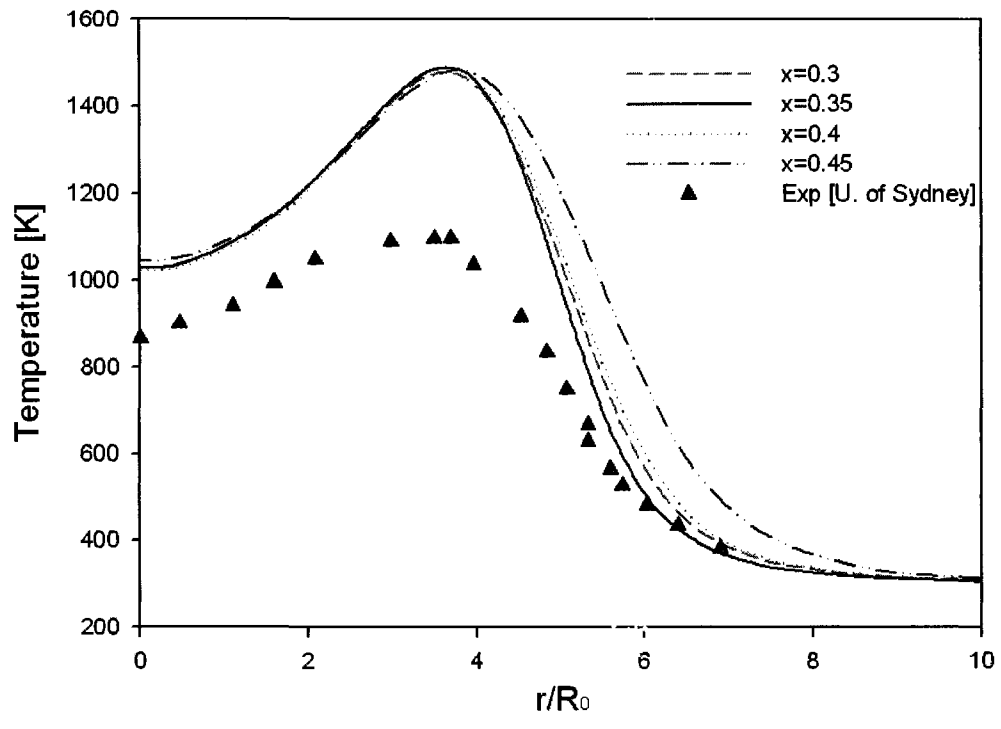| Parameter x	0.3	0.35	0.4	0.45	0.5
Time of convergence (min)	125	113	163	255	Not converged

Fig B.2 Sensitivity analysis of the computational domain at x/d=30.

APPENDIX C

SKELETAL MECHANISM

Table C.1 Skeletal Methane/air Reaction Mechanism [Smooke, 1991]

No.	Reaction	A	β	E (kJ/mole)
1f.	$H+O_2 \rightarrow OH+O$	2.000E+14	0.000	16800.
1b.	$H+O_2 \rightarrow H+O_2$	1.575E+13	0.000	690.
2f.	$O+H_2 \rightarrow OH+H$	1.800E+10	1.000	8826.
2b.	$OH+H \rightarrow O+H_2$	8.000E+09	1.000	6760.
3f.	$H_2+OH \rightarrow H_2O+H$	1.170E+09	1.300	3626.
3b.	$H_2O+H \rightarrow H_2+OH$	5.090E+09	1.300	18588.
4f.	$OH+OH \rightarrow O+H_2O$	6.000E+08	1.300	0.
4b.	$O+H_2O \rightarrow OH+OH$	5.900E+09	1.300	17029.
5.	$H+O_2+M \rightarrow HO_2+M^a$	2.300E+18	-0.800	0.
6.	$H+HO_2 \rightarrow OH+OH$	1.500E+14	0.000	1004.
7.	$H+HO_2 \rightarrow H_2+O_2$	2.500E+13	0.000	700.
8.	$OH+HO_2 \rightarrow H2O+O_2$	2.000E+13	0.000	1000.
9f.	$CO+OH \rightarrow CO_2+H$	1.510E+07	1.300	-758.
9b.	$CO_2+H \rightarrow CO+OH$	1.570E+09	1.300	22337.
10f.	$CH_4+(M) \rightarrow CH_3+H+(M)^b$	6.300E+14	0.000	104000.
10b.	$CH_3+H+(M) \rightarrow CH4+(M)^b$	5.200E+12	0.000	-1310.
11f.	$CH_4+H \rightarrow CH_3+H_2$	2.200E+04	3.000	8750.
11b.	$CH_3+H_2 \rightarrow CH_4+H$	9.570E+02	3.000	8750.
12f.	$CH_4+OH \rightarrow CH_3+H_2O$	1.600E+06	2.100	2460.
12b.	$CH_3+H_2O \rightarrow CH_4+OH$	3.020E+05	2.100	17422.
13.	$CH_3+O \rightarrow CH_2O+H$	6.800E+13	0.000	0.
14.	$CH_2O+H \rightarrow HCO+H_2$	2.500E+13	0.000	3991.
15.	$CH_2O+OH \rightarrow HCO+H_2O$	3.000E+13	0.000	1195.
16.	$HCO+H \rightarrow CO+H_2$	4.000E+13	0.000	0.
17.	$HCO+M \rightarrow CO+H+M$	1.600E+14	0.000	14700.
18.	$CH_3+O_2 \rightarrow CH_3O+O$	7.000E+12	0.000	25652.
19.	$CH_3O+H \rightarrow CH_2O+H_2$	2.000E+13	0.000	0.
20.	$CH_3O+M \rightarrow CH_2O+H+M$	2.400E+13	0.000	28812.
21.	$HO_2+HO_2 \rightarrow H_2O_2+O_2$	2.000E+12	0.000	0.
22f.	$H_2O_2+M \rightarrow OH+OH+M$	1.300E+17	0.000	45500.
22b.	$OH+OH+M \rightarrow H_2O_2+M$	9.860E+14	0.000	-5070.
23f.	$H_2O_2+OH \rightarrow H_2O+HO_2$	1.000E+13	0.000	1800.
23b.	$H_2O+HO_2 \rightarrow H_2O_2+OH$	2.860E+13	0.000	32790.
24.	$OH+H+M \rightarrow H_2O+M^a$	2.200E+22	-2.000	0.
25.	$H+H+M \rightarrow H_2+M^a$	1.800E+18	-1.000	0.

Third body efficiencies: CH_4=6.5, H_2O=6.5, CO_2 =1.5, H_2 =1.0, CO=0.75, O_2 = 0.4,

N_2 = 0.4 and all other species=1.0

The Skeletal chemical reaction mechanism, which is used in the laminar flamelet model,

is presented in Table C.1. The parameters are for the Arrhenius equation shown in Equation (C.1)

$$k_f = AT^\beta \exp(-E/RT) \qquad\qquad (C.1)$$

where A is the pre-exponential factor, E is the activation of chemical reaction, R denotes the gas constant and T is temperature (in Kelvin).

VITA AUCTORIS

Pusheng Zhang was born in 1982 in Shantou, Guangdong, P. R. China. He obtained his

Bachelor of Engineering at Nanjing University of Aeronautics and Astronautics in 2006.

Currently he is a candidate for the Master's degree in Mechanical Engineering at the

University of Windsor and hopes to graduate in summer 2008.